DOI: https://doi.org/10.17816/DD623341

Антропоморфные фантомы молочной железы для лучевой диагностики: научный обзор

Ю.А. Васильев, О.В. Омелянская, А.А. Насибуллина, Д.В. Леонов, Ю.В. Булгакова, Д.А. Ахмедзянова, Ю.Ф. Шумская, Р.В. Решетников

Научно-практический клинический центр диагностики и телемедицинских технологий, Москва, Российская Федерация

АННОТАЦИЯ

Фантомы молочной железы применяются для разработки, валидации и усовершенствования методов лучевой диагностики. В визуализации молочной железы антропоморфные модели используются для валидации, оценки и оптимизации новых методов диагностики заболеваний молочной железы, а также для контроля качества диагностических систем, совершенствования клинических протоколов и алгоритмов реконструкции изображений. Ключевым требованием к фантомам для решения этих задач является реалистичная имитация органа.

В обзоре описаны существующие на настоящий момент варианты фантомов молочной железы для лучевой диагностики и процесса их создания.

Поиск литературы, соответствующей теме обзора, производился в базах данных PubMed, eLibrary, а также в поисковой системе Google Scholar. Всего в обзор включено 72 статьи и 13 тезисов материалов конференций.

Все виды фантомов молочной железы можно разделить на два вида: вычислительные и физические. Вычислительные, в свою очередь, подразделяются на группы в зависимости от типа первичных данных: на основе математических моделей, из образцов тканей, с использований изображений медицинской визуализации молочной железы пациентки. Физические фантомы классифицируются в зависимости от способа изготовления: литья, 3D-печати или послойного формирования с использованием контрастных веществ. Основными преимуществами вычислительных фантомов являются универсальность, эффективность, точность и безопасность, а также возможность генерировать большие объёмы виртуальных данных. Физические фантомы позволяют получать наиболее реалистичные диагностические изображения без участия пациентов и проводить неограниченное число лучевых исследований.

Ключевые слова: молочная железа; 3D-печать; фантомы; фантомы для лучевой диагностики; лучевая диагностика; научный обзор.

Как цитировать:
Васильев Ю.А., Омелянская О.В., Насибуллина А.А., Леонов Д.В., Булгакова Ю.В., Ахмедзянова Д.А., Шумская Ю.Ф., Решетников Р.В. Антропоморфные фантомы молочной железы для лучевой диагностики: научный обзор // Digital Diagnostics. 2023. Т. 4, № 4. С. 569–592. DOI: https://doi.org/10.17816/DD623341

Рукопись получена: 14.11.2023 **Рукопись одобрена:** 27.11.2023 **Опубликована online:** 06.12.2023

DOI: https://doi.org/10.17816/DD623341

Anthropomorphic breast phantoms for radiology imaging: a review

Yuriy A. Vasilev, Olga V. Omelyanskaya, Anastasia A. Nasibullina, Denis V. Leonov, Julia V. Bulgakova, Dina A. Akhmedzyanova, Yuliya F. Shumskaya, Roman V. Reshetnikov

Research and Practical Clinical Center for Diagnostics and Telemedicine Technologies, Moscow, Russian Federation

ABSTRACT

Phantoms are used to validate diagnostic imaging methods or improve the skills of medical professionals. For instance, they allow conducting an unlimited number of imaging studies during medical training, assessing image quality, optimizing radiation dose, and testing novel techniques and equipment. Researchers in breast imaging use anthropomorphic models to validate, assess, and optimize new methods for diagnosing breast diseases. Such models also facilitate control over the quality of diagnostic systems, help optimize clinical protocols, and improve image reconstruction algorithms. Realistic simulation of the breast tissue is essential to address the challenges of advancing X-ray mammary gland studies. The review aimed to describe phantoms currently available for diagnostic imaging and the way they were fabricated. In this literature review, PubMed, eLIBRARY, and Google Scholar databases were screened for relevant articles. Thus, 72 articles and 13 conference papers were included. The study two major types of breast phantoms: computational and physical. Specifically, computational phantoms are classified into subgroups depending on the data they use. These include mathematical models, tissue samples, and medical images of the breast. The classification of the physical phantoms is based on their manufacturing process: casting silicone-like substances, 3D printing with resins and plastics, or printing on paper using X-ray contrast ink. Computational phantoms are generally advantageous with respect to versatility, efficiency, precision, and safety and allow the generation of large amounts of virtual data. Physical phantoms provide the most realistic diagnostic images without the need for a patient and allow performing an unlimited number of radiological studies.

Keywords: breast, 3D printing, phantoms, imaging phantoms, diagnostic radiology, literature review.

To cite this article:
Vasilev YuA, Omelyanskaya OV, Nasibullina AA, Leonov DV, Bulgakova JV, Akhmedzyanova DA, Shumskaya YuF, Reshetnikov RV. Anthropomorphic breast phantoms for radiology imaging: a review. *Digital Diagnostics.* 2023;4(4):569–592. DOI: https://doi.org/10.17816/DD623341

Received: 14.11.2023 **Accepted:** 27.11.2023 **Published online:** 06.12.2023

DOI: https://doi.org/10.17816/DD623341

用于放射诊断的仿真乳房模型：科学综述

Yuriy A. Vasilev, Olga V. Omelyanskaya, Anastasia A. Nasibullina, Denis V. Leonov, Julia V. Bulgakova, Dina A. Akhmedzyanova, Yuliya F. Shumskaya, Roman V. Reshetnikov

Research and Practical Clinical Center for Diagnostics and Telemedicine Technologies, Moscow, Russian Federation

简评

乳房模型被用于放射诊断方法的开发、验证和改进。在乳腺成像中，仿真模型被用于验证、评估和优化诊断乳腺疾病的新方法。仿真模型还被用于诊断系统的质量控制、临床协议和图像重建算法的改进。为了解决这些问题，对仿真模型的关键要求是它作为逼真的器官模拟器。

本综述旨在介绍目前可用于放射诊断的乳腺模型变体，并描述其制作过程。

我们在PubMed、eLIBRARY和Google Scholar数据库中搜索了与本综述主题有关的文献。共有72篇文章和13份会议纪要被纳入该综述。

所有类型的乳房模型可分为两类：计算模型和物理模型。计算模型又根据原始数据的类型分为几组：基于数学模型、来自组织样本、使用患者乳房的医学成像图像。物理模型则根据制作方法分为几组：铸造、3D打印或使用造影剂的逐层制作。计算模型的主要优势在于多功能性、高效性、准确性和安全性，以及生成大量虚拟数据的能力。物理模型可提供最逼真的诊断图像，无需患者参与，并对其可进行无限量的放射检查。

关键词：乳腺；3D打印；模型；用于放射诊断的模型；放射诊断；文献综述。

引用本文：

Vasilev YuA, Omelyanskaya OV, Nasibullina AA, Leonov DV, Bulgakova JV, Akhmedzyanova DA, Shumskaya YuF, Reshetnikov RV. 用于放射诊断的仿真乳房模型：科学综述. *Digital Diagnostics.* 2023;4(4):569–592. DOI: https://doi.org/10.17816/DD623341

收到： 14.11.2023 **接受：** 27.11.2023 **发布日期：** 06.12.2023

INTRODUCTION

Human phantoms are a key solution to many problematic aspects of medical imaging modalities such as ultrasonography [1], magnetic resonance imaging (MRI) [2], and computed tomography (CT) [3]. Breast phantoms (BPs) are important in the evaluation of X-ray imaging systems. They serve as a surrogate for the human body in cases where it is impractical or necessary to expose the patient to radiation. BPs are created for X-ray diagnostics to develop, optimize, and provide quality control for existing and developing imaging systems, such as full-field digital mammography (MMG), digital tomosynthesis, and CT.

Anthropomorphic BPs for X-ray diagnostics are both computational (mathematical) and physical breast models. Mathematical models describe organ structures using formulas and calculations. One of the limitations of this approach is its inability to cover the full range of anatomical variations in the breast structure and ensure its anatomical and radiological reliability. To overcome these limitations, anthropomorphic phantoms with natural distribution of different tissues were created based on segmented breast CT datasets, which guarantees a high degree of realism. Attempts to create such anthropomorphic computational phantoms have been made since the 1960s [4]. However, reliable anthropomorphic physical phantoms have only recently emerged with the advent of three-dimensional (3D)-printing technologies. The main methods for creating physical anthropomorphic MF models include casting, 3D printing, and paper-based approaches. Among these, 3D-printing technologies offer an excellent opportunity to create realistic models using materials with radiographic properties similar to those of breast tissue.

With the wider clinical use of modern quasi-3D and 3D imaging systems such as tomosynthesis and CT, physical phantoms with realistic patient anatomy are greatly needed to fully represent and evaluate the 3D behavior of such systems. In addition, considering the active and successful implementation of artificial intelligence (AI) systems in MMG analysis [5], phantoms will standardize radiographic examinations and help improve AI algorithms.

Search Methodology

PubMed and eLibrary were searched for related articles. The search terms used were selected to best reflect keywords and subject headings. PubMed search was performed using the following queries: “anthropomorphic AND breast* AND (phantom* OR phantoms, imaging [mh] OR (phantoms AND imaging) OR model*) AND (diagnostic X-ray OR radiography OR mammography OR tomography).” The eLibrary search was performed using “phantom” and “breast” keywords. Google Scholar was also used for conference proceedings search.

RESULTS

The search identified 335 papers; however, 263 papers did not meet the review criteria. The review included 72 papers and 13 conference abstracts.

Breast Anatomy

Accurate modeling of the breast using radiographic imaging requires detailed knowledge of its anatomical and radiological characteristics. The mammary gland, or the breast, is a modified cutaneous sweat gland consisting of tubuloalveolar glandular tissue, connective tissue, and other elements such as fat tissue, blood and lymphatic vessels, and nerve fibers. Most of the volume is occupied by glandular and fat tissues. Each breast is located on the fascia covering the pectoralis major muscle at the level of the III–VI ribs between the anterior axillary and parasternal lines of the corresponding side. The mammary gland is also surrounded by the anterior and posterior layers of the superficial fascia of the breast, which together form a capsule for the gland. The superficial fascia attaches to the clavicle and forms the suspensory ligament. Fibrocollagenous septa (Cooper’s ligaments) extend from the posterior layer deep into the mammary gland and from the anterior layer to the skin.

The breast comprises 15–20 lobules, which are arranged radially around the nipple and surrounded by loose connective and fatty tissue. Each lobule has its milk duct. In the subareolar region, the milk ducts widen to form lactiferous sinuses (ampullae). In these sinuses, the ducts of several lobules merge into larger ones, which exit independently into the nipple, forming separate holes on its surface. The diameter of the ducts up to the ampulla is approximately 1 mm, whereas the diameter of the main ducts varies from 2 to 4.5 mm. The total length of the ducts varies from 2 to 4.5 cm. A lobule with a diameter of 1–2 mm comprises ducts and alveoli that end in a common terminal duct. This structure is called the “terminal lobular duct unit.”

No clearly defined reference has been established for the radiographic appearance of the breast because the ratio of glandular to fatty tissue varies among women. Therefore, several classifications of mammographic density types have been developed, including Wolfe, BI-RADS, and Tabar. These classifications are shown in Table 1. BP modeling is aimed at certain categories according to the classification chosen by the researchers.

BI-RADS is the most widely used classification for describing radiographic breast density in clinical practice. The types of breast tissue structures are shown in Figure 1.

Mathematical models and diagnostic images of patients can be used to model the anatomical structures of the breast. Based on these data, three main approaches were used to create physical anthropomorphic phantoms:

- Casting methods

Table 1. Classifications of breast structure types

Type	Characteristics
	Wolfe
N1	The breast consists mainly of fat (N = normal); a low risk of breast cancer
P1	This pattern includes fat and linear densities (enlarged ducts) occupying no more than 25% of the breast; a low risk of breast cancer
P2	Linear densities (from enlarged ducts) occupying >25% of the breast. They are prominently in the upper outer quadrant but may be distributed throughout the breast (P = prominent ducts); a high risk of breast cancer
Dy	Dense breast (Dy = dysplasia); highest risk of breast cancer
Qdy	Quasi-dysplasia: this group consists of young women whose dense breasts have a somewhat spongy texture because of fatty infiltration
	BI-RADS
a	Almost entirely fat (<25% glandular density)
b	Scattered fibroglandular densities (25%–50% glandular density)
c	Heterogeneously dense (51%–75% glandular density)
d	Extremely dense (>75% glandular density)
	Tabar
I	Balanced proportion of all components of breast tissue with a slight predominance of fibrous tissue
II	Predominance of fat tissue (fat breast)
III	Predominance of fat tissue with retroareolar residual fibrous tissue
IV	Predominantly nodular density
V	Predominantly fibrous tissue (dense breast)

- Separate printing of various structures and assembling them into a complete phantom
- Printing the entire model

Computational 3D anthropomorphic models of the mammary glands

Anthropomorphic computational breast models provide anatomically reliable volumetric distribution of the radiographic absorption coefficients of different breast tissue types. Three types of approaches are available to such modeling:

1) Mathematical modeling

Phantoms based on mathematical models are designed to match certain physical or statistical properties of a human organ, such as radiographic density or statistical distribution patterns [6]. Several research groups have developed reliable model-based virtual BPs for use in projection and tomographic imaging [7–10]. An algorithm for generating this type of phantom is shown in Figure 2.

2) Tissue-based approach

These phantoms reproduce the fine-scale structure of breast tissue observed in abnormal specimens or super-resolution microtomography [11,12].

3) Approach based on the processing of patient tomograms

Such models are generated using two-dimensional (MMG) or three-dimensional (CT or MRI) images [13,14].

Mathematical breast models

This type of model is based on the modeling of the structural elements of the breast using mathematical methods. Such models comprehensively represent the shape of the organ, ductal system, Cooper's ligaments, pectoralis major muscle, blood vessels, skin, DDFM pattern, and breast abnormalities. To generate a 3D anatomically realistic model of the breast, K. Bliznakova et al. [15] and P.R. Bakic et al. [16–18] used a combination of constructive solid geometry methods and voxel techniques.

Breast model from the University of Pennsylvania

In 2002, a research group from the University of Pennsylvania developed the first anthropomorphic computational BPs based on the modeling of two ellipsoidal regions of large-scale tissue elements: predominantly fat tissue and predominantly fibroglandular tissue [16,17]. These areas are mathematically modeled using realistically distributed medium-scale phantom elements, which include the membranes, lobules, and simulated milk ducts. The duct network model is generated using a branching matrix that describes the dichotomization of tree structures [18]. The reliability of the milk duct model was evaluated by comparison with ductography data. A compression model was also developed, which reliably represents breast deformation in the University of Pennsylvania model in 2D MMG and breast tomosynthesis. Further development of this phantom consisted of adding fine structures and

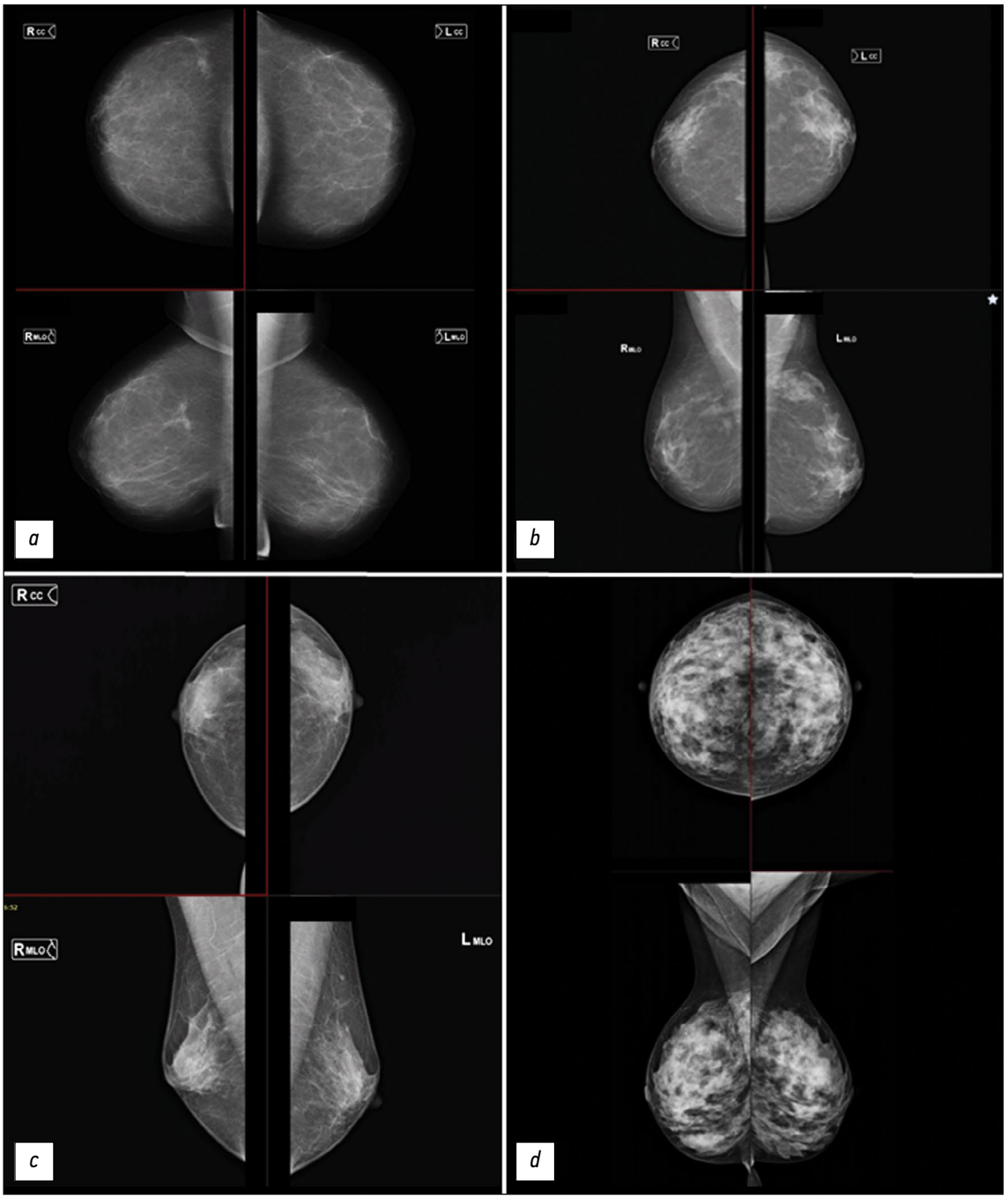

Fig. 1. Types of breast density according to the BI-RADS classification. For each image, the upper part is the craniocaudal projection, and the lower part is the mediolateral projection.

implementing an algorithm to rapidly generate high-resolution anthropomorphic phantoms with voxel sizes ranging from 25 to 1,000 μm^3 [19]. The result was an improved version of this digital phantom [12].

The proposed algorithms are based on the simplified assumption that each phantom voxel contains one tissue type. This simplification leads to the appearance of artifacts in the projection images near the boundaries between the areas of different materials, particularly at the skin–air interface. Several methods have been proposed to overcome these limitations. One of them is to model smaller voxels. However, reducing the voxel size increases the phantom generation time and the workstation requirements to simulate the phantom. Another method considers the partial volume of various tissues in a voxel [20,21]. The linear radiographic attenuation coefficient at each voxel was calculated by combining attenuation coefficients proportional to the subvolume voxels occupied by different tissues.

Breast model by the University of Patras

A research group from the University of Patras developed an anthropomorphic model of the breast, which represents

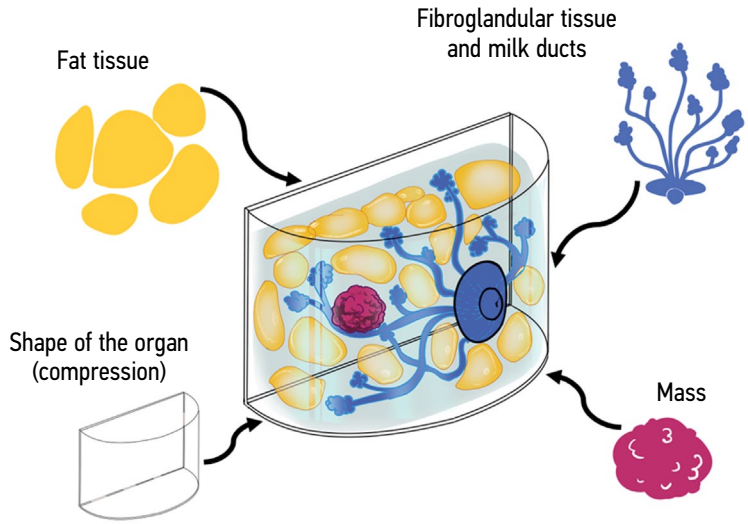

Fig. 2. An algorithm for generating a computational breast phantom.

a complex combination of anatomical shape, duct system, Cooper's ligaments, radiological tissue texture, and nodes [15]. The 3D texture simulates the presence of fatty, fibrous, and connective tissues and other tissue types that are not explicitly modeled. To obtain a realistic 3D MMG texture, a texturing algorithm based on random walk is used [10]. Cooper's ligaments are modeled as a set of thin ellipsoidal shells that appear at randomly selected points in the model. Fatty compartments are modeled by the volume of Cooper's ligaments. The pectoralis muscle is approximated as a conical object, and the nodes are modeled as round, ovoid, elongated, or irregular objects.

BPs by the United States Food and Drug Administration

Based on the above models, a research team from the United States Food and Drug Administration generated an improved, open-source, multimodal mathematical BP to be used by the scientific community [21]. Mammary glands are generated based on analytical formulas followed by voxel sampling. In this case, each voxel had an arbitrary size and consisted of one tissue type. A nipple and a 1-mm thick layer of skin are added to the front of the surface, and a layer of muscles supporting the breast is added to the back. In the inner surface, glandular sections are determined based on Voronoi segmentation. For each segmented gland compartment, a tree of ducts is grown using a random branching algorithm starting from the nipple. In the terminal branches of each "tree" of ducts, terminal lobular ducts are added. Initially, the internal part of the phantom was set as purely glandular tissue. To create subcutaneous and perilobular fat layers and some fat structures, random fat lobules should be inserted within the glandular areas. Each fat lobule is surrounded by a ligamentous structure [22]. At the final stage of phantom generation, additional structures such as blood vessels, pectoral muscles, and ligaments should be introduced.

OPTIMAM breast model

In parallel with the United States Food and Drug Administration, P. Elangovan et al. [9] presented a new method for generating quasirealistic voxel phantoms to simulate the compressed breast used in MMG and tomosynthesis. Anthropomorphic breast models were generated using a biomimetic technique with their features and structures extracted from the image planes of real breast images obtained using tomosynthesis. They are used to synthesize the 3D structure of the breast. The modeling process starts with the creation of a high-resolution blank breast model surrounded by a layer of skin. This template is populated with voxels corresponding to different tissues based on the structures extracted from the tomosynthesis images. The overall 3D shape is obtained from the tomosynthesis data using image thresholding. Then, a 1.5-mm thick layer of "skin" is added to the skin surfaces of the breast contour. Internal voxels are labeled as fat or glandular tissue.

A database of randomly selected fragments of glandular tissue was created to produce a 3D matrix of glandular tissue, which was placed in the fat tissue of the breast. The blood vessels and Cooper's ligaments are modeled as an extended 3D skeleton of the linear structures that are present in the patient's tomosynthesis images: 3–4 mm in diameter for the blood vessel network and 1–2 mm in diameter for the Cooper's ligament network.

Computational Breast Models Based on Medical Data

Several authors have attempted to create a more realistic tissue distribution in a breast model [20,23,24]. Three voxel-based breast models were generated using high-resolution segmented CT data of three compressed breasts (in three older women) [25]. These segmented breast models allowed a more realistic representation of glandular tissue and Monte Carlo calculations of the average radiation dose to

the breast during MMG and the simulation of various imaging techniques.

The development of a special breast CT system has advanced the creation of computational anthropomorphic BPs. This phantom was first developed in 2009 by CM Li et al. [14]. The key step was to develop a technique of processing breast CT scans and differentiating the breast tissue. The resulting simulated MMG image of the phantom was similar to a reliable MMG image of the breast tissue. This technique had some limitations because it did not allow for the reliable classification of small structures (Cooper's ligaments) that require higher resolution. To solve this problem, the authors proposed to express these structures mathematically and subsequently include them in the calculated breast volume.

Even though the technique by Li et al. guarantees a high degree of realism, it represents only one breast model and does not cover wide anatomical variations. To solve this problem, Hsu et al. [26,27] developed a computational technique to generate numerous anthropomorphic BPs [14]. This technique is based on morphing (a visual effect that sees one shape or object transform into another in a seamless transition) and deformation (significant distortion of shapes during digital image processing) and demonstrates the ability to create anthropomorphic BPs that are perceived as realistic by radiologists.

To enhance the development of CT-based breast models, accurate anatomical characterization of the breast using CT is required. Huang et al. [28] proposed and described in detail the anatomical features of the breast, including its shape, diameter, and length, proportion of glandular tissues in three areas of the breast, depending on the patient's age, and bra cup size. The study used the largest set of CT images of breasts available at that time (219 pieces). In addition, a research group at Duke University used them to create 224 virtual BPs [29,30]. We also developed an application to simulate different states of breast compression, allowing the use of phantoms for multimodal imaging.

Sarno et al. developed 88 computational BPs with realistic glandular tissue distribution to evaluate breast dose distribution and imaging data. These models contribute to the creation of an improved phantom that allows for a more accurate calculation of the average radiation dose to the gland during radiographic examinations [31] and optimizes tomosynthesis using virtual clinical trials.

Therefore, the main advantage of computational phantoms is their ability to generate potentially large amounts of data [21]; however, these phantoms are virtual, not physical. The quality of in silico studies depends not only on the characteristics of the virtual phantom but also on the accuracy of the simulated imaging system in representing the physical imaging modality. For example, with breast tomosynthesis or CT, virtual phantom scanning often requires detailed knowledge of the geometry of the diagnostic system and reconstruction algorithm, which is the property of the manufacturing company.

Physical anthropomorphic BPs

At the time of this review, 3D-printing technology was the most popular approach for creating physical models of breast cancer. 3D-printing technologies allow choosing printing methods and materials that resemble human tissue in density, composition, and radiographic properties. In the breast, such tissues include fat, glands, tumors, and skin.

The process of creating an anthropomorphic physical BP consists of two steps:

1) Creating a computational model of the breast using one of the methods discussed above

2) Using a computational model to produce a physical BP

Considerable efforts are being made to develop new materials because existing materials do not always have the required radiographic properties [32–34]. K. Bliznakova et al. conducted a comprehensive review of the materials used in the production of anthropomorphic models [35], and some of the main materials used to create BPs are presented in Table 2.

BPs made using casting technology

A CIRS BR3D phantom (CIRS Inc., Norfolk, USA) for MMG is produced in the form of D-shaped plates, which are connected into a single structure to form a one-piece phantom. Each plate consists of two tissue materials that simulate fat and glandular tissues in a 50:50 ratio (m/m). Two tissue-equivalent plastics are mixed to form a heterogeneous structure. Typically, several plates are produced, which can be rearranged in different orders and easily obtain different, but limited in number, variations of the underlying tissue. One of the plates contains a set of microcalcifications, fibrous tissue, and neoplasms. The phantom is used to evaluate image quality, breast tomosynthesis, and CT. The resulting images of structures on an MMG image have unclear boundaries but do not look as realistic as the patient's images. Small structures such as Cooper's ligament cannot be produced using this technology and therefore will not appear on radiographic images. In a recent study by Sage et al., the BR3D [43]-textured background was found to have high contrast and resulted in high-contrast artifacts throughout the phantom. In addition, tomosynthesis images clearly show the contours of the ring-shaped structures used to place inserts, and this phenomenon affects the results of measurements and image analysis.

An anthropomorphic BP for both X-ray and MRI was developed by Freed et al. [44] by mixing egg whites with melted refined lard and placing the resulting mixture in a breast-shaped jar. This phantom is a useful tool for quantifying image quality in 2D and 3D radiographic techniques. However, it does not allow the modeling of anatomical structures because the phantom represents them much larger than they are in the patient's body. In addition, no technique has been established for creating phantoms with sufficient glandular tissue content.

Table 2. Main materials used to produce breast phantoms for mammography.

Human tissue	Material	Density, g/cm^3
Fat tissue	Ultrahigh-molecular-weight polyethylene [36]	0.94
	Acrylonitrile butadiene styrene [32]	1.02
	PE-12 [37]	N/A
	Formlabs Clear Resin [38]	1.18
	QuickWater [33]	1.02
	Paraffin [32]	0.93
Glandular tissue	Polyvinyl alcohol (PVAL gel) [39]	1.19
	Water [40]	1.00
	Nylon [32]	1.11
	Flex polymer [32]	1.14
	TangoBlackPlus [33]	1.11
	VeroClear [33]	1.18
	VeroWhitePlus, TangoPlus Polylactin alloyed with copper and water [41]	N/A
	Polyvinyl alcohol [42]	N/A
	Formlabs gray resin [32]	1.175
Tumor tissue	Polyethylene terephthalate [42]	N/A

Ruvio et al. [45] used bread molds to create multimodal BPs for radiography, MRI, and ultrasonography imaging. The manufacturing process included five stages using three breast molds: external (replicating the breast shape), skin, and internal fibroglandular. The external shape of the breast mold follows the shape of the human breast in the supine position according to MRI data collected from patients. The main material used in the production of the skin element is a polyvinyl alcohol cryogel. The fatty structure is represented by a mixture of water and beeswax, and the fibroglandular, tumor, and muscle components are represented by agar containing a mixture of liquid (water, glycerin, and benzalkonium chloride) and dry (agar, SiC, and $Al_2 O_3$) components. The current limitation is related to the impossibility of compressing the phantom because the fat-simulating material is not susceptible and not elastic. In addition, this phantom can be stored for only 1 week because it is susceptible to bacterial damage and drying out. This results in insufficient contrast between the tumor and fibroglandular tissue. Despite the complexity of producing tissues simulating important imaging parameters across the three modalities, the study demonstrated high similarity between the reference and measured properties. This type of phantom is intended for use in multimodal cross-calibration and training when there are no living patients or cadaveric material.

BPs with integrated spherical elements

This is a special case of the approach discussed in the next subsection. Spherical elements of various sizes, made of tissue-equivalent material [46–48], are immersed into the homogeneous underlying tissue. These phantoms are widely used to assess image quality and radiation dose measurements in MMG and optimize scanning procedures in new MMG techniques such as dual-energy MMG, dual-energy contrast-enhanced MMG, tomosynthesis, and CT. A research group from the Department of Radiology of the Catholic University of Leuven developed a BP consisting of two main parts: an acrylic semicylindrical container simulating a compressed breast shape with a thickness of 58 mm and equal volumes of acrylic spheres of six different diameters [49]. Alternatively, the space between the spheres can be filled with water, a material with radiographic properties similar to those of real breast tissue. This study used an MMG system with tomosynthesis capability. Although the image pattern obtained with these phantoms differs from the actual image of the breast, they are very simple to produce and allow for easy acquisition of different views of the underlying tissue. This physical phantom has air bubbles at the top because filling the phantom completely with water is difficult. This phantom can be improved using a computational model to optimize the phantom-filling options [50–52].

K. Bliznakova et al. [53–55] have described similar approaches with semicylindrical containers printed using photopolymer resin or nylon to be filled with spheres of photopolymer resin and paraffin or animal lard as fillers. One of the versions of this approach is a small BP with a half-cylindrical shape made of Formlabs white resin. This physical phantom contains 27 Formlabs gray resin spheres with a radius of 6–13 mm, with the addition of animal fat. The phantom was used to evaluate phase-contrast imaging of the

breast [54] and develop a synthetic observer model for the quality control of tomosynthesis systems [56].

Assembling BPs from separately printed elements

This approach requires the availability of digital models of the main breast tissues, including skin, glandular, and fat tissues, as well as various neoplasms and microcalcifications. These individual digital models are based on either mathematical calculations using special computer programs [15,57] or segmentation of medical images of patients [24]. Each simulated breast tissue was saved in a separate file and then prepared for 3D printing. An example of this approach is the phantom developed by NT Dukov et al., with stereolithography used to print the external shape, network of milk ducts and neoplasms, and FDM printing using ABS filaments for fat compartments [37,53]. The selection of these printed materials is based on extensive experimental research [32,34]. The phantom is filled with water. To simulate microcalcifications, the authors used eggshells crushed into fine powder. In this case, the breast was not visualized. Further research is required to create new 3D printing materials that can simulate the radiographic properties of all types of breast tissue.

In 2016, a new version of the phantom was created with spherical insert elements [6]. Models of manually segmented breast fat compartments derived from CT images of a mastectomy specimen [22] were printed on a stereolithography 3D printer using Formlabs clear resin. Then, they were placed in a semicylindrical 48-mm-thick container filled with water, and an MMG image was obtained using a Siemens Mammomat (Siemens Healthineers, Germany). As a result, the experimental images were better than the original model; however, they were very different from the MMG images taken from the patients.

Further improvements to the compartment phantom are aimed at better similarity with patient data. This can be achieved using a less dense printing material to increase the contrast of the compartments, using smaller compartments by reducing their scale, and refining the method of segmenting the compartments. Recently, a research group from the University of Vienna developed another version of a spherical phantom consisting of VeroClear spheres with paraffin oil as a filler [58].

Printing a one-piece BP

Single media printing

The UPenn physical BP [59] is based on the mathematical model of the breast developed by the University of Pennsylvania as described above [16-18]. This technology involves the initial segmentation of digital phantom voxels into two components: fibroglandular and fat tissues. The first one was produced using a PolyJet Eden500V printer (Stratasy, USA) using tissue-equivalent material with 50% glandular tissue content (FC-720 photopolymer). Printing is performed in layers to maintain access to empty spaces, which are then filled with fat tissue equivalent. Slices are printed at 60-μm voxel resolution. The plates are then joined together to create the final anthropomorphic phantom. The initial experimental evaluation of MMG and tomosynthesis images of this physical phantom shows its potential for use in both qualitative and quantitative evaluations of the performance of 2D and 3D breast radiography systems. MMG images obtained using this phantom are visually similar to clinical images. Some limitations of this technology are related to the unclear boundaries of the structures, presence of residual air bubbles that are visible on radiographs, long manufacturing time, and high production costs.

Mainprize et al. [40,60] used a similar approach to create a two-component full-size physical BP. A voxel-based digital phantom [61] is divided into four plates to accommodate different inserts at different heights. In each plate, the fibroglandular component is removed, leaving only the fatty component. The resulting fat layer was printed using a selective laser sintering printer with a 100-μm resolution from polyamide-12. The phantom showed high similarity with data on the excess entropy parameter obtained on clinical full-fledged digital MMG.

CT and MRI scans of the breasts of individual patients are used as the basis for generating a two-chamber anthropomorphic BP proposed by Prionas et al. [62]. The glandular part consists of water, and the fatty part is made of polyethylene. 3D images are initially obtained using a special CT scan of the breast, noise is then removed, and tissue is segmented into fatty and glandular parts. The production process differs from that described above. Phantoms are produced using a numerically controlled water jet machine. A stack of breast segments was made from a 1.59-mm-thick ultrahigh-molecular-weight polyethylene sheet using a water jet machine, with the centerline of the tool path determined along the edges of the tissue structure. An outer container is molded around the thermoplastic BP, and its thickness approximately corresponds to the thickness of the skin. A container with a stack of breast segments is filled with water so that the air spaces in the phantom, which represent a glandular tissue compartment, are filled with water.

Large areas of glandular tissue in this phantom closely correspond to the original patient images. The advantage of the model is its modular design, which allows the implementation of additional objects into any glandular tissue compartment. The main limitations are related to both the technology and material used: the thickness of the polyethylene mass and the gaps between the produced breast segments resulted in the phantom being 2.6 cm longer than the patient's original breast. The characteristics of the material limit the use of the phantom in radiographic techniques where breast compression is not performed. Other minor problems are related to the presence of air bubbles in the glandular tissue, which can be removed using more complex degassing techniques during phantom assembly. Another minor concern is the waterjet cutting process, which

can also result in a reduction in the outer fat contour and an expansion of the glandular tissue contour.

2D MMG images of the patient are a key source of information in the technique of printing physical anthropomorphic BPs, as proposed and implemented by two research groups [63,64] in 2018 and 2019. A Badal et al. [63] developed an easily reproducible technique for producing anthropomorphic breast cancer models based on 2D MMG images. To produce breast objects, an Objet260 Connex3 inkjet printer (Stratasys, USA) with VeroMagenta and VeroCyan printing materials was used. The choice of this printing technology is well justified by extensive experimental data using three printers with different technologies: stereolithography, FDM modeling, and inkjet printing [65].

The key element of this approach is the mammorelocator script in the Python programing language, which calculates the thickness of the printed materials depending on the gray level of each pixel in the image and the differences in X-ray absorption between breast tissue and 3D-printing materials. Each pixel of the image is converted by the script into a column of the appropriate height.

The model was printed in 10 h, and it weighed 750 g. Currently, it is validated to correctly reproduce the radiographic properties of the breast during MMG. A study of the similarity between the original and phantom MMG showed that the anatomical features were reproduced with good accuracy. The main limitation is related to the resolution of the resulting phantom. Although the patient's initial MMG resolution is 100 μm, the 3D printer was unable to accurately reproduce the details of clinical MMG <300 μm. The authors propose using this technology to create collections of representative patient models that can be used to assess the effect of anatomical variability of the breast on the reliability of the diagnostic system.

In the study by Schophoven et al. [64], an MMG image of the breast compressed to 32 mm was used. A key challenge was to determine the pixel intensities of raw images for different thicknesses of the printed material (polypropylene) for a diverse range of clinical images. This is achieved by scanning printed plates of various thicknesses (up to 40 mm) using an MMG system. The corresponding attenuation at the pixel position of the clinical image was modeled by the height difference of the printing material, resulting in a relief-like structure on the phantom.

The phantom printing time was approximately 11 h using 791 g of RGD450 material and 31 g of auxiliary material. The described approach makes it possible to create anthropomorphic phantoms that realistically simulate the anatomy and density characteristics of the breast tissue. These phantoms can be used to solve various problems of quality control and system optimization, as well as for educational and scientific purposes. The main current limitations are related to the slightly reduced resolution of fine details compared with the original clinical image. This is due to the selected printer and material combination (PolyJet printer combined with polypropylene print material), which limits the size of the output structures to approximately 200 μm. The structures are located on the top of the phantoms; therefore, they are placed higher above the detector than the structures in the patient's breast. This can lead to increased sharpness in MMG images of denser breast tissue because of geometric magnification.

Microcalcification accumulations in this phantom were simulated using a 3D-printed base plate with a diameter of 4 mm with movable inserts and crushed eggshells [38]. The base and inserts were printed using an Objet30 Pro PolyJet 3D printer and VeroClear RGD810 material (Stratasys, USA). The base plate contained three round cavities with a diameter of 60 mm, into which rings numbered "1" to "3" were placed separately. The first ring, the "lesion ring," contains three round 10-mm cavities with corresponding covers, into which the simulated microcalcifications are placed. The other two rings are modeled as solid and do not contain any structures. All three rings have the same dimensions, which ensures their interchangeability and ability to change the position of the lesions relative to the anthropomorphic phantom. Different accumulations of microcalcifications were modeled using different amounts and sizes of eggshells.

The advantage of this approach is the modular design to integrate additional plates and rings easily and cost-effectively with different damage depending on the purpose. Phantoms made using this technology are intended for use in 2D MMG. For 3D breast imaging, physical phantoms must simulate the spatial distribution of different breast tissues in three dimensions. This can be achieved using one of the approaches discussed below.

In 2018, Okkalidis et al. [66] proposed a new technique for simultaneous printing of BPs directly from patient CT data using FDM modeling technology by changing the filling density of a homogeneous template. This template is used to accurately simulate the internal structure of the modeled 3D object. The thickest parts of the object are printed at a maximum fill density of 100%, whereas softer, lighter fabrics are printed at a lower density. This allows different types of tissue to be realistically created, considering radiological features. The method is based on reading Hounsfield units from each voxel and using these data to adjust the extrusion speed of the polylactic acid filament to obtain the required amount of extruded filament. This method was used to print an anthropomorphic BP directly using CT data [67]. The first evaluation of the phantom on a conventional CT scanner showed visual similarities between the original CT images of the patient and the phantom, which motivated the team to develop a special phantom for CT and create a future experimental setup for precision CT dosimetry. The main limitations are the long printing time (several days) and visibility of the printed pattern because of the FDM modeling technology used in the study.

Printing using two or more materials

To create ideal anthropomorphic MF phantoms, the use of different printed materials is optimal. A major step toward the realization of this goal was made in 2015 by N. Kiarashi et al. [68]. They managed to produce an anthropomorphic phantom of a compressed breast by 3D printing using two materials in parallel [26,69]. Two anthropomorphic breast models were printed using an Objet500 Connex 3D printer. The first phantom, called Doublet, was printed using two materials simultaneously, simulating glandular and fat tissues. TangoGray and VeroWhite materials were used to print the fibroglandular component. A mixture of butter and lard in a 1:1 ratio, beeswax, resin, and olive oil were studied as filler materials approaching the radiographic density of fat tissue. The resin method was repeated several times using different filling techniques, which always resulted in the presence of some unwanted air bubbles.

Physical phantoms provide a realistic radiographic view of breast anatomy in 2D and 3D images. The description of MMG physical phantoms corresponds to real human MMGs [70,71]. The disadvantages of phantoms are related to the limited dynamic range and contrast caused by the lack of suitable printing materials. This problem can be solved with the advent of new materials. Despite its limitations, the Doublet phantom has a key advantage: it has an all-in-one design, where the phantom (whole or partial) can be fabricated in one run.

AH Rossman et al. [72] reported the further development of the above-described approach to printing anthropomorphic breast models to simulate the patient's anatomy to evaluate the effectiveness of clinical MMG and digital breast tomosynthesis. They created a modular phantom with an anthropomorphic region to improve the detection of lesions and calcifications and a homogeneous region to evaluate standard quality control parameters. VeroPureWhite and a special tungsten-doped Jf flexible resin were used for fibroglandular tissue printing, and TangoPlus material and a third-party Jf flexible resin without an alloy component were used for low-density adipose tissue imaging. The design allows the addition of masses, iodized inclusions, and calcifications. One of the current limitations of this phantom is its inability to achieve BI-RADS breast radiographic density <36%. The image sensitivity depends on the radiological density: the higher the density, the lower the sensitivity of the MMG. Efforts are currently focused on achieving lower densities.

In 2019, a group from Naples [73] for the first time used an FDM 3D printer to produce physical phantoms of both uncompressed and compressed breast tissue, simulating the shape and the anatomical and radiological properties of real breast tissue. Digital phantoms based on breast CT data, and three printing materials were used to produce a physical anthropomorphic BP. Polyvinyl acetate was used to print the skin, and ABS plastic and nylon were used to print fat and glandular tissues, respectively. The skin was printed separately because computational BPs are made of three materials, and the available Ultimaker 3 FDM printer (Ultimaker, Netherlands) prints objects from a maximum of two materials. Models have 100% filling density to minimize air gaps. The internal area of the breast can be presented in the form of either printed 10-mm-thick sections or a single block of two-component material. In addition, the authors developed an area in the printed slices to accommodate TLD chips for dosimetry purposes and special holes to accommodate printed lesions [73,74].

Paper on anthropomorphic breast models

A budget-friendly way to create BPs is to use office printing paper and a regular inkjet printer [75]. Some radiopaque agents, such as potassium iodide, titanium oxide, and radiocontrast, can be used as paint additives. Parchment paper has also been tested and found to have a radiographic density similar to that of fat tissue. A physical phantom was produced using a digital model presented by Graff et al. [21] in the form of sections by inkjet printing using parchment paper and radiopaque ink containing 33% or 25% iohexol (v/v). The advantage of this approach to anthropomorphic phantom production is their low cost because they are produced using commercially available inkjet printers, inexpensive ink enhancement components, and some inexpensive additional materials. The inkjet printer used in this study was a commercially available Epson Workforce 630 desktop inkjet printer (Epson, Japan). Reusable cartridges were used instead of the original manufacturer cartridges. Because the printer has multiple color cartridges, additional "tissues" can be printed in different colors. For example, to print leather, determine the appropriate concentration of iodine ink and place it in a separate cartridge. Various colors can then be applied to the skin and glandular tissue of the image and printed accordingly.

In summary, 3D printing technology is a well-studied technique for producing anthropomorphic BPs for use in radiography [68,72]. As its main advantage, 3D printing allows the design and printing of complex structures. However, several features of the 3D-printing process limit its versatility and feasibility [41,76,77]. Although 3D printing can create products from various plastics and silicones, not all of them are amenable to the temperatures required for 3D printing. In addition, 3D printers have small printing chambers, which limits the size of the resulting features. From a practical point of view, 3D printing is an expensive and slow process and therefore impractical for high-volume production. This slowness is attributed to the time required to create anthropomorphic phantoms using 3D printing, which depends on the complexity of the design (the desired number of organic tissues and elements that must be included in the phantom structure and the desired size). In addition, postprocessing of the 3D-printed phantoms is often needed to remove the support material from the structure and smoothen the surface to achieve the desired finish. This

may include water-abrasive treatment, exposure to chemical compounds, and air-heat drying. However, these options may damage the phantoms or introduce unwanted particles into the phantoms, which could affect radiography results.

An alternative approach to creating physical phantoms is to build the model layer by layer. Each layer is a planar section. With this approach, the complexity of creating a phantom is reduced to processing 2D layers. This approach was first introduced by Theodorakou et al. [78]. In this study, each phantom layer consisted of a substrate and a contrast material (dye) applied to the substrate using a standard inkjet printer. Since then, several research groups have improved this concept and reported successful implementations [79,80]. The process of layer-by-layer generation of a phantom allows the detailed formation of radiographic density properties by adding dyes to a 2D layer; however, it has some inherent limitations. These limitations are mainly due to the dependence on the use of contrast materials (dyes). In addition to the difficulties associated with optimizing dye chemistry, the contrast material is often in a liquid state, whereas the substrate is in a solid state. Applying a liquid contrast material to a solid substrate often results in the dye bleeding into or spreading across the substrate, making it difficult to control the positioning of the contrast material. In addition, this approach usually requires multilayer application of dyes onto a single substrate, which leads to multistage drying, which negatively affects production time. Finally, inkjet printer components often cannot withstand repeated ink injections. Inkjet printers use small nozzles to deliver ink. Some contrast materials, such as iodine-based compounds, which are widely used in radiography, often lead to nozzle clogging, requiring extensive maintenance to correct process failures.

Overview of commercial phantoms

BP for MMG and tomosynthesis developed by Erler Zimmer and marketed by GTSimulators

The creation of this commercial phantom consists of two stages. Initially, a calculation model of the breast is created using the C.G. Graff method [21]. The breast surface is formed by creating a shell in the form of a quadratic hemisphere, on which a layer of skin and a nipple are applied. The shape of the shell is determined using two parameters: those that determine the total breast volume and those that correct the surface curvature. Using the Voronoi segmentation technique, the interior of the shell is randomly divided into fat and glandular components, with each glandular component containing a network of ducts with terminal lobular units. The volume is then filled with additional elements of the breast, such as Cooper's ligaments, pectoral muscles, and blood vessels. In addition, a malignant neoplasm was modeled [81], which was subsequently introduced into the model.

To create a compressed breast, its volume was converted into a four-dimensional matrix, and each element of this matrix was given elastic properties determined by voxels of the glandular or fat tissue located in the center of the element. The matrix was then formed using linear elastic finite-element modeling, and the breast was compressed in the craniocaudal direction to a thickness of 30 mm. However, no restrictions are set for creating a phantom with any breast thickness. Because the phantom model is based on analytical formulas, the compression thickness and voxel size are arbitrary. In this study, the breast model was discretized with an isotropic voxel size of 70 μm, which corresponds to the thickness of parchment paper. Depending on the size of the detector elements, undesirable effects caused by image sampling may occur at a given voxel size.

The second step is to create a physical phantom using inkjet printing. The printer used was a commercially available desktop inkjet printer (Epson Workforce 630). The print resolution was set to 363 dpi to provide a dot size of 70 μm and match the voxel size of the digital phantom (70 μm). In this procedure, special ink was applied to paper serving as background tissue to create density characteristics similar to glandular tissue. The ink was synthesized by mixing conventional pigment inks (InkThrift, Vermont PhotoInkjet, East Topsham Village, VT) with 350 mg/mL iohexol (Omnipaque, GE Healthcare, USA). One solution contains 67% ink and 33% iohexol, and the other contains 75% ink and 25% iohexol. To align the sheets, a specialized hole punch was created to make holes above the fiducial markers, and the sheets were then slid onto racks attached to a specialized backing plate to ensure that the sheets remained stationary once placed. Once the printed sheets were stacked on the base plate, a large, specialized compression paddle with post holes was placed on top of the stack to secure the sheets and ensure even compression.

To demonstrate the capabilities of the phantom, 3D lesions measuring approximately 5 mm and clusters containing microcalcifications were included in the phantom after the entire stack of sheets was manufactured. The 3D lesion was first introduced virtually and then placed into the physical phantom by reprinting the selected slices to which it extended and replacing them with nonlesional sheets at the appropriate locations. Microcalcifications were modeled by crushing eggshells and placing them at locations of varying gland densities on a physical BP. The number of elements in one cluster varied from 11 to >30. The diameter of the clusters ranged from 3.5 to 8 mm.

The materials used are similar to fat and glandular tissues in terms of radiographic density, and the production process is accurate and reproducible and can be used for both 2D and 3D imaging of the breast. In addition, this phantom is not limited to a single breast model, and any virtual model, once voxelized, can be printed using this unique approach.

This phantom has passed the validation process [75] and was used to study the capabilities of convolutional neural networks in the differential diagnosis of benign and malignant calcifications with conventional and dual-energy full-format digital MMG [84].

BR3D Breast Imaging Phantom

This phantom is described above in the section "Breast phantoms manufactured using casting technology" and is presented in Figure 3.

The model has been validated and used in many studies:

- Model-based optimization of digital breast tomosynthesis images for iterative reconstruction [83]. A new image reconstruction algorithm for digital breast tomosynthesis implemented using a total variation regularizer was tested on a Model 20 BR3D phantom. The results obtained confirm the ability of this algorithm to accurately image microcalcifications and breast formations.
- Evaluation of GPU acceleration of a model-based iterative method for digital breast tomosynthesis [84]. This study shows that parallel processing implemented on three different GPU boards allows for rapid iterative reconstruction of images obtained using digital breast tomosynthesis.

Fig. 3. BR3D Breast Imaging Phantom [82].

- Evaluation of a generative adversarial network for image quality improvement and radiation dose reduction in digital breast tomosynthesis [85]. An improvement in image quality was demonstrated during digital breast tomosynthesis under low radiation dose conditions when preprocessing the reconstruction using conditional generative adversarial networks [cGAN (pix2pix)].

Other BPs

Commercial BPs are available; however, data on their use in scientific research are unavailable. They include the following:

- Model 011A by CIRS is a tissue-equivalent anthropomorphic phantom designed to test the performance of all types of MMG systems. Models of calcifications, ducts, and neoplasms were built into the phantom as test objects. The sizes of the test objects vary, which allows testing the system at different levels of complexity. The resin material simulates the photon attenuation coefficients of various breast tissues. The average elemental composition of the simulated tissue was based on the individual elemental composition of fat and glandular tissues. This phantom has been used in some studies aimed at improving the accuracy of diagnostic methods [86–88]. The phantom is shown in Figure 4.
- BT-A01 by True Phantom Solutions (Canada) is a life-size image of a female torso, carefully crafted to reflect typical anatomical features. It is used for MMG, CT, and MRI. The target audience is healthcare professionals and students.
- Complex Breast Phantom SynAtomy 160,650 by SynDaver (USA) is an anthropomorphic breast phantom intended for training students and medical personnel. Modalities include ultrasonography, elastography, and MMG.

CONCLUSION

This study provides a brief historical overview of the development and use of anthropomorphic breast models for radiography. Different approaches to creating such phantoms have both advantages and limitations. Depending on the specific medical imaging task, one or the other approach may be preferred. Although computational anthropomorphic phantoms offer anatomical fidelity and relative ease of modeling, the creation of physical anthropomorphic models is challenging. Available technologies are costly and labor intensive, and the range of materials used is limited. Although much work has been done in this area, searching for new materials with X-ray absorption coefficients that correspond to different types of breast tissue is necessary. In addition, low-cost production technologies are also needed. This will improve and accelerate the production of anthropomorphic BPs for radiography.

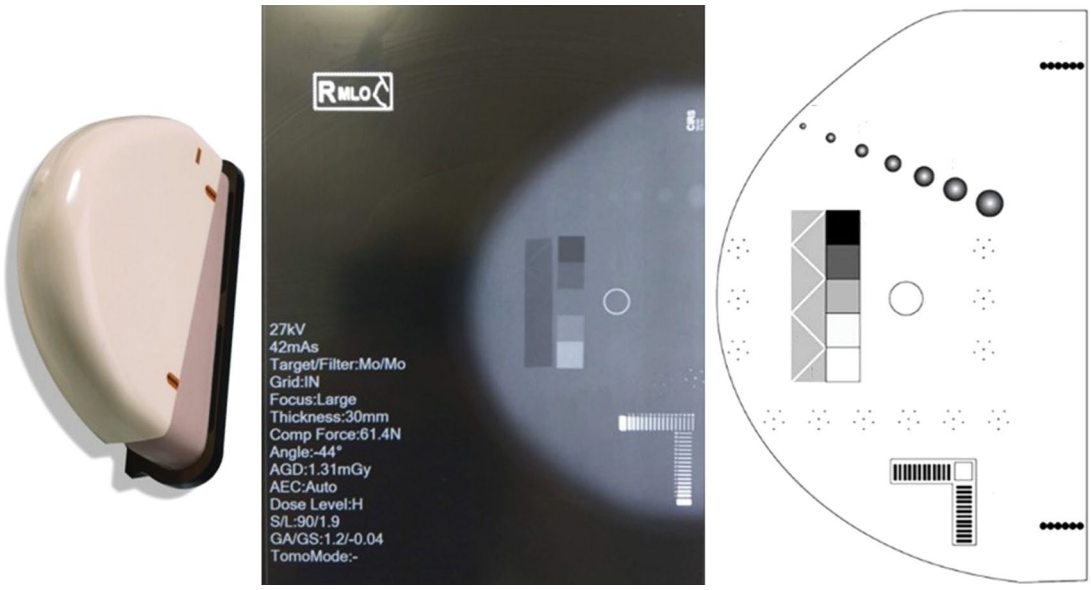

Fig. 4. 011A by CIRS.

ADDITIONAL INFORMATION

Funding source. This article was prepared by a group of authors as a part of the research and development effort titled "Scientific rationale for development and use of tissue-equivalent materials to design test objects for radiology" (USIS No.: № 123092000013-3) in accordance with the Order No. 1196 dated December 21, 2022 "On approval of state assignments funded by means of allocations from the budget of the city of Moscow to the state budgetary (autonomous) institutions subordinate to the Moscow Health Care Department, for 2023 and the planned period of 2024 and 2025" issued by the Moscow Health Care Department.

Competing interests. The authors declare that they have no competing interests.

Authors' contribution. All authors made a substantial contribution to the conception of the work, acquisition, analysis, interpretation of data for the work, drafting and revising the work, final approval of the version to be published and agree to be accountable for all aspects of the work. Yuriy A. Vasilev — conception and design of the study, data analysis, approval of the final version of the article; Olga V. Omelyanskaya — conception and design of the study, editing, approval of the final version of the article; Anastasia A. Nasibullina — text writing, data collection and processing, data analysis; Denis V. Leonov — data collection and processing, data analysis, editing; Julia V. Bulgakova — text writing, data analysis; Dina A. Akhmedzyanova — text writing, data collection and processing, literature review; Yuliya F. Shumskaya — text writing, data collection and processing, literature review; Roman V. Reshetnikov — conception and design of the study, literature review, editing, approval of the final version of the article.

REFERENCES

1. Leonov D, Venidiktova D, Costa-Júnior JFS, et al. Development of an anatomical breast phantom from polyvinyl chloride plastisol with lesions of various shape, elasticity and echogenicity for teaching ultrasound examination. *International Journal of Computer Assisted Radiology and Surgery.* 2023. doi: 10.1007/s11548-023-02911-4

2. Nuzov NB, Bhusal B, Henry KR, et al. True location of deep brain stimulation electrodes differs from what is seen on postoperative magnetic resonance images: An anthropomorphic phantom study. *Annual International Conference of the IEEE Engineering in Medicine and Biology Society. IEEE Engineering in Medicine and Biology Society.* 2022:1863–1866. doi: 10.1109/EMBC48229.2022.9871619

3. Cannella R, Shahait M, Furlan AA, et al. Efficacy of single-source rapid kV-switching dual-energy CT for characterization of non-uric acid renal stones: a prospective ex vivo study using anthropomorphic phantom. *Abdominal Radiology.* 2020;45(4):1092–1099. doi: 10.1007/s00261-019-02164-3

4. Kramer R, Zankl M, Williams G, Drexler G, et al. *The calculation of dose from external photon exposures using reference human phantoms and Monte Carlo methods.* 1982.

5. Vasilev YA, Tyrov IA, Vladzymyrskyy AV, et al. Double-reading mammograms using artificial intelligence technologies: A new model of mass preventive examination organization. *Digital Diagnostics.* 2023;4(2):93–104. doi: 10.17816/DD321423

6. Cockmartin L, Bosmans H, Marshall NW. Comparative power law analysis of structured breast phantom and patient images in digital mammography and breast tomosynthesis. *Medical physics.* 2013;40(8):081920. doi: 10.1118/1.4816309

7. Ma AKW, Gunn S, Darambara DG. Introducing DeBRa: a detailed breast model for radiological studies. *Physics in medicine and biology.* 2009;54(14):4533–4545. doi: 10.1088/0031-9155/54/14/010

8. Chen B, Shorey J, Saunders RS, et al. An Anthropomorphic Breast Model for Breast Imaging Simulation and Optimization. *Academic radiology.* 2011;18(5):536–546. doi: 10.1016/j.acra.2010.11.009

9. Elangovan P, Mackenzie A, Dance DR, et al. Design and validation of realistic breast models for use in multiple alternative forced choice virtual clinical trials. *Physics in medicine and biology.* 2017;62(7):2778–2794. doi: 10.1088/1361-6560/aa622c
10. Bliznakova K, Suryanarayanan S, Karellas A, Pallikarakis N. Evaluation of an improved algorithm for producing realistic 3D breast software phantoms: Application for mammography. *Medical Physics.* 2010;37(11):5604–5617. doi: 10.1118/1.3491812
11. O'Connor JM, Das M, Dider C, Mahd M, Glick SJ. Generation of voxelized breast phantoms from surgical mastectomy specimens. *Medical Physics.* 2013;40(4). doi: 10.1118/1.4795758
12. Lau BA, Reiser I, Nishikawa RM. A statistically defined anthropomorphic software breast phantom. *Medical Physics.* 2012;39(6):3375–3385. doi: 10.1118/1.4718576
13. Sarno A, Mettivier G, di Franco F, et al. Dataset of patient-derived digital breast phantoms for in silico studies in breast computed tomography, digital breast tomosynthesis, and digital mammography. *Medical Physics.* 2021;48(5):2682–2693. doi: 10.1002/mp.14826
14. Li CM, Segars WP, Tourassi GD, Boone JM, Dobbins JT. Methodology for generating a 3D computerized breast phantom from empirical data. *Medical Physics.* 2009;36(7):3122–3131. doi: 10.1118/1.3140588
15. Bliznakova K, Bliznakov Z, Bravou V, Kolitsi Z, Pallikarakis N. A three-dimensional breast software phantom for mammography simulation. *Physics in medicine and biology.* 2003;48(22):3699–3719. doi: 10.1088/0031-9155/48/22/006
16. Bakic PR, Albert M, Brzakovic D, Maidment AD. Mammogram synthesis using a 3D simulation. I. Breast tissue model and image acquisition simulation. *Medical Physics.* 2002;29(9):2131–2139. doi: 10.1118/1.1501143
17. Bakic PR, Albert M, Brzakovic D, Maidment AD. Mammogram synthesis using a 3D simulation. II. Evaluation of synthetic mammogram texture. *Medical Physics.* 2002;29(9):2140–2151. doi: 10.1118/1.1501144
18. Bakic PR, Albert M, Brzakovic D, Maidment AD. Mammogram synthesis using a three-dimensional simulation. III. Modeling and evaluation of the breast ductal network. *Medical Physics.* 2003;30(7):1914–1925. doi: 10.1118/1.1586453
19. Pokrajac DD, Maidment ADA, Bakic PR. Optimized generation of high resolution breast anthropomorphic software phantoms. *Medical Physics.* 2012;39(4):2290–2302. doi: 10.1118/1.3697523
20. Chen F, Pokrajac D, Shi X, et al. Partial volume simulation in software breast phantoms. *Medical Imaging 2012: Physics of Medical Imaging.* 2012. doi: 10.1117/12.912242
21. Graff CG. A new, open-source, multi-modality digital breast phantom. *Proceedings of the SPIE.* 2016;9783. doi: 10.1117/12.2216312
22. Ikejimba LC, Salad J, Graff CG, et al. A four-alternative forced choice (4AFC) methodology for evaluating microcalcification detection in clinical full-field digital mammography (FFDM) and digital breast tomosynthesis (DBT) systems using an inkjet-printed anthropomorphic phantom. *Medical Physics.* 2019;46(9):3883–3892. doi: 10.1002/mp.13629
23. Imran A-A-Z, Bakic PR, Pokrajac DD. Spatial distribution of adipose compartments size, shape and orientation in a CT breast image of a mastectomy specimen. *2015 IEEE Signal Processing in Medicine and Biology Symposium (SPMB).* 2015:1–2. doi: 10.1109/SPMB.2015.7405460
24. Imran A-A-Z, Pokrajac DD, Maidment ADA, Bakic PR. Estimation of adipose compartment volumes in CT images of a mastectomy specimen. *Proceedings of the SPIE.* 2016;9783. doi: 10.1117/12.2217175
25. Hoeschen C, Fill U, Zankl M, et al. A high-resolution voxel phantom of the breast for dose calculations in mammography. *Radiation protection dosimetry.* 2005;114(1–3):406–409. doi: 10.1093/rpd/nch558
26. Hsu CM, Palmeri ML, Segars WP, Veress AI, Dobbins JT. An analysis of the mechanical parameters used for finite element compression of a high-resolution 3D breast phantom. *Medical Physics.* 2011;38(10):5756–5770. doi: 10.1118/1.3637500
27. Hsu CML, Palmeri ML, Segars WP, Veress AI, Dobbins JT. Generation of a suite of 3D computer-generated breast phantoms from a limited set of human subject data. *Medical Physics.* 2013;40(4). doi: 10.1118/1.4794924
28. Huang SY, Boone JM, Yang K, et al. The characterization of breast anatomical metrics using dedicated breast CT. *Medical Physics.* 2011;38(4):2180–2191. doi: 10.1118/1.3567147
29. Segars WP, Veress AI, Wells JR, et al. Population of 100 realistic, patient-based computerized breast phantoms for multi-modality imaging research. *Proceedings of the SPIE.* 2014;9033. doi: 10.1117/12.2043868
30. Erickson DW, Wells JR, Sturgeon GM, et al. Population of 224 realistic human subject-based computational breast phantoms. *Medical Physics.* 2015;43(1):23–32. doi: 10.1118/1.4937597
31. Sarno A, Mettivier G, Di Lillo F, et al. Homogeneous vs. patient specific breast models for Monte Carlo evaluation of mean glandular dose in mammography. *Physica Medica.* 2018;51:56–63. doi: 10.1016/j.ejmp.2018.04.392
32. Ivanov D, Bliznakova K, Buliev I, et al. Suitability of low density materials for 3D printing of physical breast phantoms. *Physics in medicine and biology.* 2018;63(17). doi: 10.1088/1361-6560/aad315
33. Santos JC, Almeida CD, Iwahara A, Peixoto JE. Characterization and applicability of low-density materials for making 3D physical anthropomorphic breast phantoms. *Radiation Physics and Chemistry.* 2019;164. doi: 10.1016/j.radphyschem.2019.108361
34. Esposito G, Mettivier G, Bliznakova K, et al. Investigation of the refractive index decrement of 3D printing materials for manufacturing breast phantoms for phase contrast imaging. *Physics in medicine and biology.* 2019;64(7). doi: 10.1088/1361-6560/ab0670
35. Bliznakova K, Buliev I, Bliznakov Z. *Anthropomorphic Phantoms in Image Quality and Patient Dose Optimization.* Philadelphia: IOP Publishing; 2018. doi: 10.1088/2053-2563/aae197
36. Hernandez AM, Seibert JA, Nosratieh A, Boone JM. Generation and analysis of clinically relevant breast imaging x-ray spectra. *Medical Physics.* 2017;44(6):2148–2160. doi: 10.1002/mp.12222
37. Dukov NT, Feradov FN, Gospodinova GD, Bliznakova KS. An Approach for Printing Tissue-mimicking Abnormalities Dedicated to Applications in Breast Imaging. *2019 IEEE XXVIII International Scientific Conference Electronics (ET).* 2019:1–4. doi: 10.1109/ET.2019.8878587
38. Mäder U, Martin F, Karin B, Stephan S. Concept to extend anthropomorphic breast phantoms for 2D digital mammography with movable lesions at variable reproducible positions. *15th International Workshop on Breast Imaging (IWBI2020).* 2020. doi: 10.1117/12.2560619
39. Okoh FO, Kabir NA, Mohd FMY, Siti NAA. Measurement of mass attenuation coefficient of polyvinyl alcohol (PVAL) as breast

tissue equivalent material in the photon energy range of 16.61–25.26 keV. *Journal of Physics: Conference Series.* 2020;1535(1). doi: 10.1088/1742-6596/1535/1/012051

40. Mainprize JG, Mawdsley GE, Carton A-K, et al. Full-size anthropomorphic phantom for 2D and 3D breast x-ray imaging. *Proceedings of the SPIE.* 2020;11513:17. doi: 10.1117/12.2560358

41. Filippou V, Tsoumpas C. Recent advances on the development of phantoms using 3D printing for imaging with CT, MRI, PET, SPECT, and ultrasound. *Medical Physics.* 2018;45(9):e740–e760. doi: 10.1002/mp.13058

42. di Franco F, Mettivier G, Sarno A, Varallo A, Russo P. Manufacturing of physical breast phantoms with 3D printing technology for X-ray breast imaging. *2019 IEEE Nuclear Science Symposium and Medical Imaging Conference (NSS/MIC).* 2019:1–5. doi: 10.1109/NSS/MIC42101.2019.9059986

43. Sage J, Fezzani KL, Fitton I, et al. Experimental evaluation of seven quality control phantoms for digital breast tomosynthesis. *Physica Medica.* 2019;57:137–144. doi: 10.1016/j.ejmp.2018.12.031

44. Freed M, Badal A, Jennings RJ, et al. X-ray properties of an anthropomorphic breast phantom for MRI and x-ray imaging. *Physics in medicine and biology.* 2011;56(12):3513–3533. doi: 10.1088/0031-9155/56/12/005

45. Ruvio G, Solimene R, Cuccaro A, et al. Multimodal Breast Phantoms for Microwave, Ultrasound, Mammography, Magnetic Resonance and Computed Tomography Imaging. *Sensors.* 2020;20(8):2400. doi: 10.3390/s20082400

46. Baldelli P, Phelan N, Egan G. Investigation of the effect of anode/filter materials on the dose and image quality of a digital mammography system based on an amorphous selenium flat panel detector. *Br J Radiol.* 2010;83(988):290–295. doi: 10.1259/bjr/60404532

47. Park S, Jennings R, Liu H, Badano A, Myers K. A statistical, task-based evaluation method for three-dimensional x-ray breast imaging systems using variable-background phantoms. *Medical Physics.* 2010;37(12):6253–6270. doi: 10.1118/1.3488910

48. Taibi A, Fabbri S, Baldelli P, et al. Dual-energy imaging in full-field digital mammography: a phantom study. *Physics in medicine and biology.* 2003;48(13):1945–1956. doi: 10.1088/0031-9155/48/13/307

49. Cockmartin L, Marshall N, Bosmans H. Design and Evaluation of a Phantom with Structured Background for Digital Mammography and Breast Tomosynthesis. In: Maidment ADA, Bakic PR, Gavenonis S, editors. *Breast Imaging. IWDM 2012. Lecture Notes in Computer Science, vol 7361.* Berlin: Springer; 2012. doi: 10.1007/978-3-642-31271-7_83

50. Baneva Y, Bliznakova K, Cockmartin L, et al. Evaluation of a breast software model for 2D and 3D X-ray imaging studies of the breast. *Physica Medica.* 2017;41:78–86. doi: 10.1016/j.ejmp.2017.04.024

51. Bliznakova K. Development of breast software phantom dedicated for research and educational purposes. *RAD Association Journal.* 2017;2(1):14–19. doi: 10.21175/RadJ.2017.01.004

52. Marinov S, Carton A-K, Cockmartin L, et al. Evaluation of the visual realism of breast texture phantoms in digital mammography. *Proc. SPIE 11513, 15th International Workshop on Breast Imaging (IWBI2020).* 2020. doi: 10.1117/12.2564124

53. Feradov F, Marinov S, Bliznakova K. Physical Breast Phantom Dedicated for Mammography Studies. In: Henriques J, Neves N, de Carvalho P, editors. *XV Mediterranean Conference on Medical and Biological Engineering and Computing – MEDICON 2019. MEDICON 2019. IFMBE Proceedings.* 2020;76:344–352. doi: 10.1007/978-3-030-31635-8_41

54. Bliznakova K, Mettivier G, Russo P, Bliznakov Zh. Validation of a software platform for 2D and 3D phase contrast imaging: preliminary subjective evaluation. *15th International Workshop on Breast Imaging (IWBI2020).* 2020:97. doi: 10.1117/12.2564356

55. Bliznakova K, Mettivier G, Russo P, et al. A software platform for phase contrast x-ray breast imaging research. *Comput Biol Med.* 2015;61:62–74. doi: 10.1016/j.compbiomed.2015.03.017

56. Petrov D, Marshall NW, Young KC, Bosmans H. Systematic approach to a channelized Hotelling model observer implementation for a physical phantom containing mass-like lesions: Application to digital breast tomosynthesis. *Physica Medica.* 2019;58:8–20. doi: 10.1016/j.ejmp.2018.12.033

57. Mettivier G, Bliznakova K, Sechopoulos I, et al. Evaluation of the BreastSimulator Software Platform for Breast Tomography: Preliminary Results. *Physics in Medicine and Biology.* 2016;62(16):145–151. doi: 10.1088/1361-6560/aa6ca3

58. Salomon E, Semturs F, Unger E, et al. Equivalent breast thickness and dose sensitivity of a next iteration 3D structured breast phantom with lesion models. *Medical Imaging 2020: Physics of Medical Imaging.* 2020. doi: 10.1117/12.2548956

59. Carton AK, Bakic P, Ullberg C, Derand H, Maidment AD. Development of a physical 3D anthropomorphic breast phantom. *Medical Physics.* 2011;38(2):891–896. doi: 10.1118/1.3533896

60. Mainprize JG, Carton A-K, Klausz R, et al. Development of a physical 3D anthropomorphic breast texture model using selective laser sintering rapid prototype printing. *Medical Imaging 2018: Physics of Medical Imaging.* 2018:9. doi: 10.1117/12.2560358

61. Li Z, Desolneux A, Muller S, Carton A-K. A Novel 3D Stochastic Solid Breast Texture Model for X-Ray Breast Imaging. In: Tingberg A, Lång K, Timberg P, editors. *Breast Imaging. IWDM 2016. Lecture Notes in Computer Science, vol 9699.* Springer; 2016. P. 660–667. doi: 10.1007/978-3-319-41546-8_822016

62. Prionas ND, Burkett GW, McKenney SE, et al. Development of a patient-specific two-compartment anthropomorphic breast phantom. *Physics in medicine and biology.* 2012;57(13):4293–4307. doi: 10.1088/0031-9155/57/13/4293

63. Badal A, Clark M, Ghammraoui B. Reproducing two-dimensional mammograms with three-dimensional printed phantoms. *Journal of Medical Imaging.* 2018;5(3). doi: 10.1117/1.JMI.5.3.033501

64. Schopphoven S, Cavael P, Bock K, Fiebich M, Mäder U. Breast phantoms for 2D digital mammography with realistic anatomical structures and attenuation characteristics based on clinical images using 3D printing. *Physics in medicine and biology.* 2019;64(21). doi: 10.1088/1361-6560/ab3f6a

65. Clark M, Ghammraoui B, Badal A. Reproducing 2D breast mammography images with 3D printed phantoms. *Medical Imaging 2016: Physics of Medical Imaging.* 2016;9783. doi: 10.1117/12.2217215

66. Okkalidis N. A novel 3D printing method for accurate anatomy replication in patient-specific phantoms. *Medical Physics.* 2018;45(10):4600–4606. doi: 10.1002/mp.13154

67. Daskalov S, Okkalidis N, Boone JM, et al. Anthropomorphic Physical Breast Phantom Based on Patient Breast CT Data: Preliminary Results. In: Henriques J, Neves N, de Carvalho P, editors. *XV Mediterranean Conference on Medical and Biological Engineering and Computing – MEDICON 2019. MEDICON 2019. IFMBE Proceedings, vol 76.* Springer; 2020. P. 367–374. doi: 10.1007/978-3-030-31635-8_442020

68. Kiarashi N, Nolte AC, Sturgeon GM, et al. Development of realistic physical breast phantoms matched to virtual breast phantoms based on human subject data. *Medical Physics.* 2015;42(7):4116–4126. doi: 10.1118/1.4919771
69. Lindfors KK, Boone JM, Nelson TR, et al. Dedicated Breast CT: Initial Clinical Experience. *Radiology.* 2008;246(3):725–733. doi: 10.1148/radiol.2463070410
70. Burgess AE, Judy PF. Signal detection in power-law noise: effect of spectrum exponents. *Journal of the Optical Society of America A.* 2007;24(12):B52–B60. doi: 10.1364/JOSAA.24.000B52
71. Burgess AE, Jacobson FL, Judy PF. Human observer detection experiments with mammograms and power-law noise. *Medical Physics.* 2001;28(4):419–437. doi: 10.1118/1.1355308
72. Rossman AH, Catenacci M, Zhao C, et al. Three-dimensionally-printed anthropomorphic physical phantom for mammography and digital breast tomosynthesis with custom materials, lesions, and uniform quality control region. *Journal of Medical Imaging.* 2019;6(2). doi: 10.1117/1.JMI.6.2.021604
73. Mettivier G, Sarno A, Boone JM, et al. Virtual clinical trials in 3D and 2D breast imaging with digital phantoms derived from clinical breast CT scans. *Medical Imaging 2020: Physics of Medical Imaging.* 2020. doi: 10.1117/12.2548224
74. Mettivier G, Sarno A, di Franco F, et al. The Napoli-Varna-Davis project for virtual clinical trials in X-ray breast imaging. *2019 IEEE Nuclear Science Symposium and Medical Imaging Conference (NSS/MIC).* 2019:1–5. doi: 10.1109/NSS/MIC42101.2019.9059828
75. Ikejimba LC, Graff CG, Rosenthal S, et al. A novel physical anthropomorphic breast phantom for 2D and 3D x-ray imaging. *Medical Physics.* 2017;44(2):407–416. doi: 10.1002/mp.12062
76. Mei K, Geagan M, Roshkovan L, et al. Three-dimensional printing of patient-specific lung phantoms for CT imaging: Emulating lung tissue with accurate attenuation profiles and textures. *Medical Physics.* 2022;49(2):825–835. doi: 10.1002/mp.15407
77. Ionita CN, Mokin M, Varble N, et al. Challenges and limitations of patient-specific vascular phantom fabrication using 3D Polyjet printing. *Proceedings of SPIE--the International Society for Optical Engineering.* doi: 10.1117/12.2042266
78. Theodorakou C, Horrocks JA, Marshall NW, Speller RD. A novel method for producing x-ray test objects and phantoms. *Physics in medicine and biology.* 2004;49(8):1423–1438. doi: 10.1088/0031-9155/49/8/004
79. Sikaria D, Musinsky S, Sturgeon GM, et al. Second generation anthropomorphic physical phantom for mammography and DBT: Incorporating voxelized 3D printing and inkjet printing of iodinated lesion inserts. *Proc. SPIE 9783, Medical Imaging 2016: Physics of Medical Imaging.* 2016. doi: 10.1117/12.2217667
80. Jahnke P, Limberg FR, Gerbl A, et al. Radiopaque Three-dimensional Printing: A Method to Create Realistic CT Phantoms. *Radiology.* 2017;282(2):569–575. doi: 10.1148/radiol.2016152710
81. de Sisternes L, Brankov JG, Zysk AM, et al. A computational model to generate simulated three-dimensional breast masses. *Medical Physics.* 2015;42(2):1098–1118. doi: 10.1118/1.4905232
82. SUN NUCLEAR. BR3D BREAST IMAGING PHANTOM [Internet] [cited 1 Jan 2023]. Available from: https://www.cirsinc.com/products/mammography/br3d-breast-imaging-phantom/
83. Piccolomini EL, Morotti E. A Model-Based Optimization Framework for Iterative Digital Breast Tomosynthesis Image Reconstruction. *Journal of imaging.* 2021;7(2):36. doi: 10.3390/jimaging7020036
84. Cavicchioli R, Hu JC, Loli Piccolomini E, Morotti E, Zanni L. GPU acceleration of a model-based iterative method for Digital Breast Tomosynthesis. *Scientific reports.* 2020;10(1):43. doi: 10.1038/s41598-019-56920-y
85. Gomi T, Kijima Y, Kobayashi T, Koibuchi Y. Evaluation of a Generative Adversarial Network to Improve Image Quality and Reduce Radiation-Dose during Digital Breast Tomosynthesis. *Diagnostics.* 2022;12(2):495. doi: 10.3390/diagnostics12020495
86. Cockmartin L, Bosmans H, Marshall NW. Establishing a quality control protocol for dual-energy based contrast-enhanced digital mammography. *Proceedings of the SPIE.* 2021;11595. doi: 10.1117/12.2581816
87. Marimón E, Marsden PA, Nait-Charif H, Díaz O. A semi-empirical model for scatter field reduction in digital mammography. *Physics in medicine and biology.* 2021;66(4). doi: 10.1088/1361-6560/abd231
88. Silver EH, Shulman SD, Rehani MM. Innovative monochromatic x-ray source for high-quality and low-dose medical imaging. *Medical Physics.* 2021;48(3):1064–1078. doi: 10.1002/mp.14677

СПИСОК ЛИТЕРАТУРЫ

1. Leonov D., Venidiktova D., Costa-Júnior J.F.S., et al. Development of an anatomical breast phantom from polyvinyl chloride plastisol with lesions of various shape, elasticity and echogenicity for teaching ultrasound examination // International Journal of Computer Assisted Radiology and Surgery. 2023. doi: 10.1007/s11548-023-02911-4
2. Nuzov N.B., Bhusal B., Henry K.R., et al. True location of deep brain stimulation electrodes differs from what is seen on postoperative magnetic resonance images: An anthropomorphic phantom study // Annual International Conference of the IEEE Engineering in Medicine and Biology Society. IEEE Engineering in Medicine and Biology Society. 2022. P. 1863–1866. doi: 10.1109/EMBC48229.2022.9871619
3. Cannella R., Shahait M., Furlan A.A., et al. Efficacy of single-source rapid kV-switching dual-energy CT for characterization of non-uric acid renal stones: a prospective ex vivo study using anthropomorphic phantom // Abdominal Radiology. 2020. Vol. 45, N 4. P. 1092–1099. doi: 10.1007/s00261-019-02164-3
4. Kramer R., Zankl M., Williams G., Drexler G., et al. The calculation of dose from external photon exposures using reference human phantoms and Monte Carlo methods. 1982.
5. Васильев Ю.А., Тыров И.А., Владзимирский А.В., и др. Двойной просмотр результатов маммографии с применением технологий искусственного интеллекта: новая модель организации массовых профилактических исследований // Digital Diagnostics. 2023. Т. 4, № 2. С. 93–104. doi: 10.17816/DD3214236.
6. Cockmartin L., Bosmans H., Marshall N.W. Comparative power law analysis of structured breast phantom and patient images in digital mammography and breast tomosynthesis // Med Phys. 2013. Vol. 40, № 8. P. 81920.
7. Ma A.K.W., Gunn S., Darambara D.G. Introducing DeBRa: a detailed breast model for radiological studies // Physics in medicine and biology. 2009. Vol. 54, N 14. P. 4533–4545. doi: 10.1088/0031-9155/54/14/010

8. Chen B., Shorey J., Saunders R.S., et al. An Anthropomorphic Breast Model for Breast Imaging Simulation and Optimization // Academic radiology. 2011. Vol. 18, N 5. P. 536–546. doi: 10.1016/j.acra.2010.11.009
9. Elangovan P., Mackenzie A., Dance D.R., et al. Design and validation of realistic breast models for use in multiple alternative forced choice virtual clinical trials // Physics in medicine and biology. 2017. Vol. 62, N 7. P. 2778–2794. doi: 10.1088/1361-6560/aa622c
10. Bliznakova K., Suryanarayanan S., Karellas A., Pallikarakis N. Evaluation of an improved algorithm for producing realistic 3D breast software phantoms: Application for mammography // Medical Physics. 2010. Vol. 37, N 11. P. 5604–5617. doi: 10.1118/1.3491812
11. O'Connor J.M., Das M., Dider C., Mahd M., Glick S.J. Generation of voxelized breast phantoms from surgical mastectomy specimens // Medical Physics. 2013. Vol. 40, N 4. doi: 10.1118/1.4795758
12. Lau B.A., Reiser I., Nishikawa R.M. A statistically defined anthropomorphic software breast phantom // Medical Physics. 2012. Vol. 39, N 6. P. 3375–3385. doi: 10.1118/1.4718576
13. Sarno A., Mettivier G., di Franco F., et al. Dataset of patient-derived digital breast phantoms for in silico studies in breast computed tomography, digital breast tomosynthesis, and digital mammography // Medical Physics. 2021. Vol. 48, N 5. P. 2682–2693. doi: 10.1002/mp.14826
14. Li C.M., Segars W.P., Tourassi G.D., Boone J.M., Dobbins J.T. Methodology for generating a 3D computerized breast phantom from empirical data // Medical Physics. 2009. Vol. 36, N 7. P. 3122–3131. doi: 10.1118/1.3140588
15. Bliznakova K., Bliznakov Z., Bravou V., Kolitsi Z., Pallikarakis N. A three-dimensional breast software phantom for mammography simulation // Physics in medicine and biology. 2003. Vol. 48, N 22. P. 3699–3719. doi: 10.1088/0031-9155/48/22/006
16. Bakic P.R., Albert M., Brzakovic D., Maidment A.D. Mammogram synthesis using a 3D simulation. I. Breast tissue model and image acquisition simulation // Medical Physics. 2002. Vol. 29, N 9. P. 2131–2139. doi: 10.1118/1.1501143
17. Bakic P.R., Albert M., Brzakovic D., Maidment A.D. Mammogram synthesis using a 3D simulation. II. Evaluation of synthetic mammogram texture // Medical Physics. 2002. Vol. 29, N 9. P. 2140–2151. doi: 10.1118/1.1501144
18. Bakic P.R., Albert M., Brzakovic D., Maidment A.D. Mammogram synthesis using a three-dimensional simulation. III. Modeling and evaluation of the breast ductal network // Medical Physics. 2003. Vol. 30, N 7. P. 1914–1925. doi: 10.1118/1.1586453
19. Pokrajac D.D., Maidment A.D.A., Bakic P.R. Optimized generation of high resolution breast anthropomorphic software phantoms // Medical Physics. 2012. Vol. 39, N 4. P. 2290–2302. doi: 10.1118/1.3697523
20. Chen F., Pokrajac D., Shi X., et al. Partial volume simulation in software breast phantoms // Medical Imaging 2012: Physics of Medical Imaging. 2012. doi: 10.1117/12.912242
21. Graff C.G. A new, open-source, multi-modality digital breast phantom // Proceedings of the SPIE. 2016. Vol. 9783. doi: 10.1117/12.2216312
22. Ikejimba L.C., Salad J., Graff C.G., et al. A four-alternative forced choice (4AFC) methodology for evaluating microcalcification detection in clinical full-field digital mammography (FFDM) and digital breast tomosynthesis (DBT) systems using an inkjet-printed anthropomorphic phantom // Medical Physics. 2019. Vol. 46, N 9. P. 3883–3892. doi: 10.1002/mp.13629
23. Imran A.-A.-Z., Bakic P.R., Pokrajac D.D. Spatial distribution of adipose compartments size, shape and orientation in a CT breast image of a mastectomy specimen // 2015 IEEE Signal Processing in Medicine and Biology Symposium (SPMB). 2015. P. 1–2. doi: 10.1109/SPMB.2015.7405460
24. Imran A.-A.-Z., Pokrajac D.D., Maidment A.D.A., Bakic P.R. Estimation of adipose compartment volumes in CT images of a mastectomy specimen // Proceedings of the SPIE. 2016. Vol. 9783. doi: 10.1117/12.2217175
25. Hoeschen C., Fill U., Zankl M., et al. A high-resolution voxel phantom of the breast for dose calculations in mammography // Radiation protection dosimetry. 2005. Vol. 114, N 1–3. P. 406–409. doi: 10.1093/rpd/nch558
26. Hsu C.M., Palmeri M.L., Segars W.P., Veress A.I., Dobbins J.T. An analysis of the mechanical parameters used for finite element compression of a high-resolution 3D breast phantom // Medical Physics. 2011. Vol. 38, N 10. P. 5756–5770. doi: 10.1118/1.3637500
27. Hsu C.M.L., Palmeri M.L., Segars W.P., Veress A.I., Dobbins J.T. Generation of a suite of 3D computer-generated breast phantoms from a limited set of human subject data // Medical Physics. 2013. Vol. 40, N 4. doi: 10.1118/1.4794924
28. Huang S.Y., Boone J.M., Yang K., et al. The characterization of breast anatomical metrics using dedicated breast CT // Medical Physics. 2011. Vol. 38, N 4. P. 2180–2191. doi: 10.1118/1.3567147
29. Segars W.P., Veress A.I., Wells J.R., et al. Population of 100 realistic, patient-based computerized breast phantoms for multi-modality imaging research // Proceedings of the SPIE. 2014. Vol. 9033. doi: 10.1117/12.2043868
30. Erickson D.W., Wells J.R., Sturgeon G.M., et al. Population of 224 realistic human subject-based computational breast phantoms // Medical Physics. 2015. Vol. 43, N 1. P. 23–32. doi: 10.1118/1.4937597
31. Sarno A., Mettivier G., Di Lillo F., et al. Homogeneous vs. patient specific breast models for Monte Carlo evaluation of mean glandular dose in mammography // Physica Medica. 2018. Vol. 51. P. 56–63. doi: 10.1016/j.ejmp.2018.04.392
32. Ivanov D., Bliznakova K., Buliev I., et al. Suitability of low density materials for 3D printing of physical breast phantoms // Physics in medicine and biology. 2018. Vol. 63, N 17. doi: 10.1088/1361-6560/aad315
33. Santos J.C., Almeida C.D., Iwahara A., Peixoto J.E. Characterization and applicability of low-density materials for making 3D physical anthropomorphic breast phantoms // Radiation Physics and Chemistry. 2019. Vol. 164. doi: 10.1016/j.radphyschem.2019.108361
34. Esposito G., Mettivier G., Bliznakova K., et al. Investigation of the refractive index decrement of 3D printing materials for manufacturing breast phantoms for phase contrast imaging // Physics in medicine and biology. 2019. Vol. 64, N 7. doi: 10.1088/1361-6560/ab0670
35. Bliznakova K., Buliev I., Bliznakov Z. Anthropomorphic Phantoms in Image Quality and Patient Dose Optimization. Philadelphia : IOP Publishing, 2018. doi: 10.1088/2053-2563/aae197
36. Hernandez A.M., Seibert J.A., Nosratieh A., Boone J.M. Generation and analysis of clinically relevant breast imaging x-ray spectra // Medical Physics. 2017. Vol. 44, N 6. P. 2148–2160. doi: 10.1002/mp.12222
37. Dukov N.T., Feradov F.N., Gospodinova G.D., Bliznakova K.S. An Approach for Printing Tissue-mimicking Abnormalities Dedicated to Applications in Breast Imaging // 2019 IEEE XXVIII

International Scientific Conference Electronics (ET). 2019. P. 1–4. doi: 10.1109/ET.2019.8878587

38. Mäder U., Martin F., Karin B., Stephan S. Concept to extend anthropomorphic breast phantoms for 2D digital mammography with movable lesions at variable reproducible positions // 15th International Workshop on Breast Imaging (IWBI2020). 2020. doi: 10.1117/12.2560619

39. Okoh F.O., Kabir N.A., Mohd F.M.Y., Siti N.A.A. Measurement of mass attenuation coefficient of polyvinyl alcohol (PVAL) as breast tissue equivalent material in the photon energy range of 16.61–25.26 keV // Journal of Physics: Conference Series. 2020. Vol. 1535, N 1. doi: 10.1088/1742-6596/1535/1/012051

40. Mainprize J.G., Mawdsley G.E., Carton A.-K., et al. Full-size anthropomorphic phantom for 2D and 3D breast x-ray imaging // Proceedings of the SPIE. 2020. Vol. 11513. P. 17. doi: 10.1117/12.2560358

41. Filippou V., Tsoumpas C. Recent advances on the development of phantoms using 3D printing for imaging with CT, MRI, PET, SPECT, and ultrasound // Medical Physics. 2018. Vol. 45, N 9. P. e740–e760. doi: 10.1002/mp.13058

42. di Franco F., Mettivier G., Sarno A., Varallo A., Russo P. Manufacturing of physical breast phantoms with 3D printing technology for X-ray breast imaging // 2019 IEEE Nuclear Science Symposium and Medical Imaging Conference (NSS/MIC). 2019. P. 1–5. doi: 10.1109/NSS/MIC42101.2019.9059986

43. Sage J., Fezzani K.L., Fitton I., et al. Experimental evaluation of seven quality control phantoms for digital breast tomosynthesis // Physica Medica. 2019. Vol. 57. P. 137–144. doi: 10.1016/j.ejmp.2018.12.031

44. Freed M., Badal A., Jennings R.J., et al. X-ray properties of an anthropomorphic breast phantom for MRI and x-ray imaging // Physics in medicine and biology. 2011. Vol. 56, N 12. P. 3513–3533. doi: 10.1088/0031-9155/56/12/005

45. Ruvio G., Solimene R., Cuccaro A., et al. Multimodal Breast Phantoms for Microwave, Ultrasound, Mammography, Magnetic Resonance and Computed Tomography Imaging // Sensors. 2020. Vol. 20, N 8. P. 2400. doi: 10.3390/s20082400

46. Baldelli P., Phelan N., Egan G. Investigation of the effect of anode/filter materials on the dose and image quality of a digital mammography system based on an amorphous selenium flat panel detector // Br J Radiol. 2010. Vol. 83, N 988. P. 290–295. doi: 10.1259/bjr/60404532

47. Park S., Jennings R., Liu H., Badano A., Myers K. A statistical, task-based evaluation method for three-dimensional x-ray breast imaging systems using variable-background phantoms // Medical Physics. 2010. Vol. 37, N 12. P. 6253–6270. doi: 10.1118/1.3488910

48. Taibi A., Fabbri S., Baldelli P., et al. Dual-energy imaging in full-field digital mammography: a phantom study // Physics in medicine and biology. 2003. Vol. 48, N 13. P. 1945–1956. doi: 10.1088/0031-9155/48/13/307

49. Cockmartin L., Marshall N., Bosmans H. Design and Evaluation of a Phantom with Structured Background for Digital Mammography and Breast Tomosynthesis. In: Maidment A.D.A., Bakic P.R., Gavenonis S., editors. Breast Imaging. IWDM 2012. Lecture Notes in Computer Science, vol 7361. Berlin : Springer, 2012. doi: 10.1007/978-3-642-31271-7_83

50. Baneva Y., Bliznakova K., Cockmartin L., et al. Evaluation of a breast software model for 2D and 3D X-ray imaging studies of the breast // Physica Medica. 2017. Vol. 41. P. 78–86. doi: 10.1016/j.ejmp.2017.04.024

51. Bliznakova K. Development of breast software phantom dedicated for research and educational purposes // RAD Association Journal. 2017. Vol. 2, N 1. P. 14–19. doi: 10.21175/RadJ.2017.01.004

52. Marinov S., Carton A.-K., Cockmartin L., et al. Evaluation of the visual realism of breast texture phantoms in digital mammography // Proc. SPIE 11513, 15th International Workshop on Breast Imaging (IWBI2020). 2020. doi: 10.1117/12.2564124

53. Feradov F., Marinov S., Bliznakova K. Physical Breast Phantom Dedicated for Mammography Studies. In: Henriques J., Neves N., de Carvalho P., editors. XV Mediterranean Conference on Medical and Biological Engineering and Computing – MEDICON 2019. MEDICON 2019. IFMBE Proceedings, vol 76. Springer, 2020. P. 344–352. doi: 10.1007/978-3-030-31635-8_41

54. Bliznakova K., Mettivier G., Russo P., Bliznakov Zh. Validation of a software platform for 2D and 3D phase contrast imaging: preliminary subjective evaluation // 15th International Workshop on Breast Imaging (IWBI2020). 2020. P. 97. doi: 10.1117/12.2564356

55. Bliznakova K., Mettivier G., Russo P., et al. A software platform for phase contrast x-ray breast imaging research // Comput Biol Med. 2015. Vol. 61. P. 62–74. doi: 10.1016/j.compbiomed.2015.03.017

56. Petrov D., Marshall N.W., Young K.C., Bosmans H. Systematic approach to a channelized Hotelling model observer implementation for a physical phantom containing mass-like lesions: Application to digital breast tomosynthesis // Physica Medica. 2019. Vol. 58. P. 8–20. doi: 10.1016/j.ejmp.2018.12.033

57. Mettivier G., Bliznakova K., Sechopoulos I., et al. Evaluation of the BreastSimulator Software Platform for Breast Tomography: Preliminary Results // Physics in Medicine and Biology. 2016. Vol. 62, N 16. P. 145–151. doi: 10.1088/1361-6560/aa6ca3

58. Salomon E., Semturs F., Unger E., et al. Equivalent breast thickness and dose sensitivity of a next iteration 3D structured breast phantom with lesion models // Medical Imaging 2020: Physics of Medical Imaging. 2020. doi: 10.1117/12.2548956

59. Carton A.-K., Bakic P., Ullberg C., Derand H., Maidment A.D. Development of a physical 3D anthropomorphic breast phantom // Medical Physics. 2011. Vol. 38, N 2. P. 891–896. doi: 10.1118/1.3533896

60. Mainprize J.G., Carton A.-K., Klausz R., et al. Development of a physical 3D anthropomorphic breast texture model using selective laser sintering rapid prototype printing // Medical Imaging 2018: Physics of Medical Imaging. 2018. P. 9. doi: 10.1117/12.2560358

61. Li Z., Desolneux A., Muller S., Carton A.-K. A Novel 3D Stochastic Solid Breast Texture Model for X-Ray Breast Imaging. In: Tingberg A., Lång K., Timberg P., editors. Breast Imaging. IWDM 2016. Lecture Notes in Computer Science, vol 9699. Springer, 2016. P. 660–667. doi: 10.1007/978-3-319-41546-8_822016

62. Prionas N.D., Burkett G.W., McKenney S.E., et al. Development of a patient-specific two-compartment anthropomorphic breast phantom // Physics in medicine and biology. 2012. Vol. 57, N 13. P. 4293–4307. doi: 10.1088/0031-9155/57/13/4293

63. Badal A., Clark M., Ghammraoui B. Reproducing two-dimensional mammograms with three-dimensional printed phantoms // Journal of Medical Imaging. 2018. Vol. 5, N 3. doi: 10.1117/1.JMI.5.3.033501

64. Schopphoven S., Cavael P., Bock K., Fiebich M., Mäder U. Breast phantoms for 2D digital mammography with realistic anatomical structures and attenuation characteristics based on clinical images

using 3D printing // Physics in medicine and biology. 2019. Vol. 64, N 21. doi: 10.1088/1361-6560/ab3f6a
65. Clark M., Ghammraoui B., Badal A. Reproducing 2D breast mammography images with 3D printed phantoms // Medical Imaging 2016: Physics of Medical Imaging. 2016. Vol. 9783. doi: 10.1117/12.2217215
66. Okkalidis N. A novel 3D printing method for accurate anatomy replication in patient-specific phantoms // Medical Physics. 2018. Vol. 45, N 10. P. 4600–4606. doi: 10.1002/mp.13154
67. Daskalov S., Okkalidis N., Boone J.M., et al. Anthropomorphic Physical Breast Phantom Based on Patient Breast CT Data: Preliminary Results. In: Henriques J., Neves N., de Carvalho P., editors. XV Mediterranean Conference on Medical and Biological Engineering and Computing – MEDICON 2019. MEDICON 2019. IFMBE Proceedings, vol 76. Springer, 2020. P. 367–374. doi: 10.1007/978-3-030-31635-8_442020
68. Kiarashi N., Nolte A.C., Sturgeon G.M., et al. Development of realistic physical breast phantoms matched to virtual breast phantoms based on human subject data // Medical Physics. 2015. Vol. 42, N 7. P. 4116–4126. doi: 10.1118/1.4919771
69. Lindfors K.K., Boone J.M., Nelson T.R., et al. Dedicated Breast CT: Initial Clinical Experience // Radiology. 2008. Vol. 246, N 3. P. 725–733. doi: 10.1148/radiol.2463070410
70. Burgess A.E., Judy P.F. Signal detection in power-law noise: effect of spectrum exponents // Journal of the Optical Society of America A. 2007. Vol. 24, N 12. P. B52–B60. doi: 10.1364/JOSAA.24.000B52
71. Burgess A.E., Jacobson F.L., Judy P.F. Human observer detection experiments with mammograms and power-law noise // Medical Physics. 2001. Vol. 28, N 4. P. 419–437. doi: 10.1118/1.1355308
72. Rossman A.H., Catenacci M., Zhao C., et al. Three-dimensionally-printed anthropomorphic physical phantom for mammography and digital breast tomosynthesis with custom materials, lesions, and uniform quality control region // Journal of Medical Imaging. 2019. Vol. 6, N 2. doi: 10.1117/1.JMI.6.2.021604
73. Mettivier G., Sarno A., Boone J.M., et al. Virtual clinical trials in 3D and 2D breast imaging with digital phantoms derived from clinical breast CT scans // Medical Imaging 2020: Physics of Medical Imaging. 2020. doi: 10.1117/12.2548224
74. Mettivier G., Sarno A, di Franco F., et al. The Napoli-Varna-Davis project for virtual clinical trials in X-ray breast imaging // 2019 IEEE Nuclear Science Symposium and Medical Imaging Conference (NSS/MIC). 2019. P. 1–5. doi: 10.1109/NSS/MIC42101.2019.9059828
75. Ikejimba L.C., Graff C.G., Rosenthal S., et al. A novel physical anthropomorphic breast phantom for 2D and 3D x-ray imaging // Medical Physics. 2017. Vol. 44, N 2. P. 407–416. doi: 10.1002/mp.12062
76. Mei K., Geagan M., Roshkovan L., et al. Three-dimensional printing of patient-specific lung phantoms for CT imaging: Emulating lung tissue with accurate attenuation profiles and textures // Medical Physics. 2022. Vol. 49, N 2. P. 825–835. doi: 10.1002/mp.15407
77. Ionita C.N., Mokin M., Varble N., et al. Challenges and limitations of patient-specific vascular phantom fabrication using 3D Polyjet printing // Proceedings of SPIE--the International Society for Optical Engineering. doi: 10.1117/12.2042266
78. Theodorakou C., Horrocks J.A., Marshall N.W., Speller R.D. A novel method for producing x-ray test objects and phantoms // Physics in medicine and biology. 2004. Vol. 49, N 8. P. 1423–1438. doi: 10.1088/0031-9155/49/8/004
79. Sikaria D., Musinsky S., Sturgeon G.M., et al. Second generation anthropomorphic physical phantom for mammography and DBT: Incorporating voxelized 3D printing and inkjet printing of iodinated lesion inserts. Proc. SPIE 9783, Medical Imaging 2016: Physics of Medical Imaging. 2016. doi: 10.1117/12.2217667
80. Jahnke P., Limberg F.R., Gerbl A., et al. Radiopaque Three-dimensional Printing: A Method to Create Realistic CT Phantoms // Radiology. 2017. Vol. 282, N 2. P. 569–575. doi: 10.1148/radiol.2016152710
81. de Sisternes L., Brankov J.G., Zysk A.M., et al. A computational model to generate simulated three-dimensional breast masses // Medical Physics. 2015. Vol. 42, N 2. P. 1098–1118. doi: 10.1118/1.4905232
82. SUN NUCLEAR. BR3D BREAST IMAGING PHANTOM [Internet] [дата обращения 01.01.2023]. Доступ по ссылке: https://www.cirsinc.com/products/mammography/br3d-breast-imaging-phantom/
83. Piccolomini E.L., Morotti E. A Model-Based Optimization Framework for Iterative Digital Breast Tomosynthesis Image Reconstruction // Journal of imaging. 2021. Vol. 7, N 2. P. 36. doi: 10.3390/jimaging7020036
84. Cavicchioli R., Hu J.C., Loli Piccolomini E., Morotti E., Zanni L. GPU acceleration of a model-based iterative method for Digital Breast Tomosynthesis // Scientific reports. 2020. Vol. 10, N 1. P. 43. doi: 10.1038/s41598-019-56920-y
85. Gomi T., Kijima Y., Kobayashi T., Koibuchi Y. Evaluation of a Generative Adversarial Network to Improve Image Quality and Reduce Radiation-Dose during Digital Breast Tomosynthesis // Diagnostics. 2022. Vol. 12, N 2. P. 495. doi: 10.3390/diagnostics1202049586.
86. Cockmartin L., Bosmans H., Marshall N.W. Establishing a quality control protocol for dual-energy based contrast-enhanced digital mammography // Proceedings of the SPIE. 2021. Vol. 11595. doi: 10.1117/12.2581816
87. Marimón E., Marsden P.A., Nait-Charif H., Díaz O. A semi-empirical model for scatter field reduction in digital mammography // Physics in medicine and biology. 2021. Vol. 66, N 4. doi: 10.1088/1361-6560/abd231
88. Silver E.H., Shulman S.D., Rehani M.M. Innovative monochromatic x-ray source for high-quality and low-dose medical imaging // Medical Physics. 2021. Vol. 48, N 3. P. 1064–1078. doi: 10.1002/mp.14677

AUTHORS' INFO

*** Anastasia A. Nasibullina;**
address: 24/1 Petrovka street, 127051, Moscow, Russia
ORCID: 0000-0003-1695-7731;
eLibrary SPIN: 2482-3372;
e-mail: NasibullinaAA@zdrav.mos.ru

ОБ АВТОРАХ

*** Насибуллина Анастасия Александровна;**
адрес: Россия, 127051, Москва, ул.Петровка, д.24, стр. 1;
ORCID: 0000-0003-1695-7731;
eLibrary SPIN: 2482-3372;
e-mail: NasibullinaAA@zdrav.mos.ru

* Corresponding author / Автор, ответственный за переписку

Yuriy A. Vasilev, MD, Cand. Sci. (Med.);
ORCID: 0000-0002-5283-5961;
eLibrary SPIN: 4458-5608;
e-mail: VasilevYA1@zdrav.mos.ru

Olga V. Omelyanskaya;
ORCID: 0000-0002-0245-4431;
eLibrary SPIN: 8948-6152;
e-mail: OmelyanskayaOV@zdrav.mos.ru

Denis V. Leonov, Cand. Sci. (Tech.);
ORCID: 0000-0003-0916-6552;
eLibrary SPIN: 5510-4075;
e-mail: LeonovDV2@zdrav.mos.ru

Julia V. Bulgakova;
ORCID: 0000-0002-1627-6568;
eLibrary SPIN: 8945-6205;
e-mail: BulgakovaYV@zdrav.mos.ru

Dina A. Akhmedzyanova, MD;
ORCID: 0000-0001-7705-9754;
eLibrary SPIN: 6983-5991;
e-mail: AkhmedzyanovaDA@zdrav.mos.ru

Yuliya F. Shumskaya, MD;
ORCID: 0000-0002-8521-4045;
eLibrary SPIN: 3164-5518;
e-mail: shumskayayf@zdrav.mos.ru

Roman V. Reshetnikov, Cand. Sci. (Phys. and Math.);
ORCID: 0000-0002-9661-0254;
eLibrary SPIN: 8592-0558;
e-mail: r.reshetnikov@npcmr.ru

Васильев Юрий Александрович, канд. мед. наук;
ORCID: 0000-0002-5283-5961;
eLibrary SPIN: 4458-5608;
e-mail: VasilevYA1@zdrav.mos.ru

Омелянская Ольга Васильевна;
ORCID: 0000-0002-0245-4431;
eLibrary SPIN: 8948-6152;
e-mail: OmelyanskayaOV@zdrav.mos.ru

Леонов Денис Владимирович, канд. техн. наук;
ORCID: 0000-0003-0916-6552;
eLibrary SPIN: 5510-4075;
e-mail: LeonovDV2@zdrav.mos.ru

Булгакова Юлия Владиславовна;
ORCID: 0000-0002-1627-6568;
eLibrary SPIN: 8945-6205;
e-mail: BulgakovaYV@zdrav.mos.ru

Ахмедзянова Дина Альфредовна;
ORCID: 0000-0001-7705-9754;
eLibrary SPIN: 6983-5991;
e-mail: AkhmedzyanovaDA@zdrav.mos.ru

Шумская Юлия Федоровна;
ORCID: 0000-0002-8521-4045;
eLibrary SPIN: 3164-5518;
e-mail: shumskayayf@zdrav.mos.ru

Решетников Роман Владимирович, канд. ф.-м. наук;
ORCID: 0000-0002-9661-0254;
eLibrary SPIN: 8592-0558;
e-mail: r.reshetnikov@npcmr.ru